REMOVAL OF DISINFECTION BY-PRODUCTS IN WATER BY
ADSORPTION ON THIOL-FUNCTIONALIZED MESOPOROUS MATERIAL

Miss Yaowalak Krueyai

A Thesis Submitted in Partial Fulfillment of the Requirements

for the Degree of Master of Science Program in Environmental Management

(Interdisciplinary Program)

Graduate School

Chulalongkorn University

Academic Year 2014

การกำจัดสารพลอยได้จากกระบวนการฆ่าเชื้อโรคในน้ำ
โดยการดูดซับบนวัสดุรูพรุนที่ต่อติดหมู่ไทออล

นางสาวเยาวลักษณ์ เครือใย

Thesis Title	REMOVAL OF DISINFECTION BY-PRODUCTS IN WATER BY ADSORPTION ON THIOL-FUNCTIONALIZED MESOPOROUS MATERIAL
By	Miss Yaowalak Krueyai
Field of Study	Environmental Management
Thesis Advisor	Aunnop Wongrueng, Ph.D.
Thesis Co-Advisor	Associate Professor Patiparn Punyapalakul, Ph.D.

Accepted by the Graduate School, Chulalongkorn University in Partial Fulfillment of the Requirements for the Master's Degree

....Dean of the Graduate School
(Associate Professor Sunait Chutintaranond, Ph.D.)

THESIS COMMITTEE

....Chairman
(Assistant Professor Srilert Chotpantarat, Ph.D.)
....Thesis Advisor
(Aunnop Wongrueng, Ph.D.)
....Thesis Co-Advisor
(Associate Professor Patiparn Punyapalakul, Ph.D.)
....Examiner
(Associate Professor Chawalit Ngamcharussrivichai, Ph.D.)
....External Examiner
(Panida Prarat, Ph.D.)

เยาวลักษณ์ เครือใย : การกำจัดสารพลอยได้จากกระบวนการฆ่าเชื้อโรคในน้ำโดยการดูดซับบนวัสดุรู พรุนที่ต่อติดหมู่ไทออล (REMOVAL OF DISINFECTION BY-PRODUCTS IN WATER BY ADSORPTION ON THIOL-FUNCTIONALIZED MESOPOROUS MATERIAL) อ.ที่ ปรึกษาวิทยานิพนธ์หลัก: อ. ดร. อรรณพ วงศ์เรือง, อ.ที่ปรึกษาวิทยานิพนธ์ร่วม: รศ. ดร. ปฏิภาณ ปัญญาพลกุล, 93 หน้า.

วัตถุประสงค์หลักของงานวิจัยนี้คือการศึกษาการกำจัดสารพลอยได้จากกระบวนการฆ่าเชื้อโรคในน้ำ โดยการดูดซับบนวัสดุรูพรุนที่ต่อติดหมู่ไทออล ตัวดูดซับที่มีรูพรุนที่ต่อติดหมู่ไทออลอยู่บนพื้นฐานของยาง ธรรมชาติและเมโซพอรัสซิลิเกต (NR/HMS-SH) ถูกสังเคราะห์เพื่อศึกษาประสิทธิภาพและกลไกการดูดซับ เปรียบเทียบกับถ่านกัมมันต์ชนิดผง (PAC) การอธิบายลักษณะผลการวิเคราะห์พบหมู่ฟังก์ชั่นของตัวดูดซับ และ ปริมาณกำมะถันในตัวดูดซับยืนยันการปรากฏตัวของกลุ่มไทออลโดยการวิเคราะห์ธาตุ การเลี้ยวเบนของรังสี เอ็กซ์ถูกนำมาใช้ในการประเมินโครงสร้างผลึกและวิเคราะห์โครงสร้างของตัวดูดซับ นอกจากนี้จลนพลศาสตร์ ของการดูดซับและรูปแบบไอโซเทอมถูกนำมาใช้ในการกำหนดกลไกการดูดซับ การดูดซับแบบคัดเลือกของ NR/HMS-SH ในน้ำประปาได้รับการตรวจสอบผลที่ได้ชี้ให้เห็นว่าการดูดซับบน NR/HMS-SH และผงถ่านกัม มันต์ของไดคลอโรอะซิโตรไนไตรล์ (DCAN) ไตรคลอโรมีเทน (TCM) และไตรคลอโรอะซิโตน (C$_3$H$_3$Cl$_3$O) มีประสิทธิภาพการดูดซับสูงกว่าไดคลอโรอะซิติก เอซิด (DCAA) นอกจากนี้โครงสร้างโมเลกุลที่แตกต่างกัน ของกลุ่มฮาโลอะซิโตรไนไตรล์ (HANs) และแรงทางประจุไฟฟ้าระหว่างไอออนและขั้วใน TCM และ C$_3$H$_3$Cl$_3$O ส่งผลต่อประสิทธิภาพการดูดซับและสมบัติการดูดซับแบบคัดเลือกในสารละลายเดี่ยวและ สารละลายผสม นอกจากนี้ผลของสารอินทรีย์ธรรมชาติ (NOM) แสดงให้เห็นว่าส่วนที่ไม่ชอบน้ำ (HPO) NOM ทำให้ความสามารถในการดูดซับของการดูดซับ DCAN บนวัสดุสังเคราะห์ลดลง ในขณะที่ส่วนที่ชอบน้ำ (HPI) NOM ไม่ได้ลดสมบัติการดูดซับบนตัวดูดซับสังเคราะห์ลง อาจจะเป็นสาเหตุมาจากการแข่งขันของการดูดซับบน พื้นผิวตัวดูดซับ

สาขาวิชา การจัดการสิ่งแวดล้อม   ลายมือชื่อนิสิต _____
ปีการศึกษา 2557   ลายมือชื่อ อ.ที่ปรึกษาหลัก _____
                                        ลายมือชื่อ อ.ที่ปรึกษาร่วม _____

5687581620 : MAJOR ENVIRONMENTAL MANAGEMENT

KEYWORDS: DISINFECTION BY-PRODUCTS / ADSORPTION / COMPOSITE MATERIAL

YAOWALAK KRUEYAI: REMOVAL OF DISINFECTION BY-PRODUCTS IN WATER BY ADSORPTION ON THIOL-FUNCTIONALIZED MESOPOROUS MATERIAL. ADVISOR: AUNNOP WONGRUENG, Ph.D., CO-ADVISOR: ASSOC. PROF. PATIPARN PUNYAPALAKUL, Ph.D., 93 pp.

The main objective of this research is to study the removal of disinfection by-product (DBPs) in water by adsorption on thiol-functionalized mesoporous material. Thiol-functionalized mesoporous composite based on natural rubber and hexagonal mesoporous silica (NR/HMS-SH) was synthesized to investigate adsorption efficiency and mechanism compared with powder activated carbon (PAC). Fourier-transform infrared spectroscopy (FTIR) results revealed the functional group of NR/HMS-SH and the sulfur content that confirming the presence of thiol group was measured by elemental analyzer. X-ray diffraction (XRD) was used to evaluate crystalline structure and analyze the structure of NR/HMS-SH. Moreover, adsorption kinetics and isotherm models were used to determine the adsorption mechanism and the adsorption selectivity of adsorbent on adsorption of DBPs in tap water was investigated. The result indicated that adsorption onto the NR/HMS-SH and PAC of dichloroacetronitrile (DCAN), trichloromethane (TCM) and 1,1,1-trichloroacetone ($C_3H_3Cl_3O$) presence the higher adsorption capacity than dichloroacetic acid (DCAA). Furthermore, the different molecular structure of HANs and the ion-dipole electrostatic interaction of TCM and $C_3H_3Cl_3O$ affected the adsorption capacity and selectivity in both of single and mixed solute. In addition, the result of natural organic carbon (NOM) showed that the hydrophobic (HPO) NOM decreased the adsorption capacity of DCAN adsorption on synthesized material while hydrophilic (HPI) NOM did not prefer the decreasing of adsorption capacity on NR/HMS-SH. It might be cause of the adsorption competition on adsorbent surface.

Field of Study: Environmental Management	Student's Signature	....
Academic Year: 2014	Advisor's Signature	....
	Co-Advisor's Signature	....

ACKNOWLEDGEMENTS

CONTENTS

ABBREVIATIONS

DBPs	Disinfection by-products
DCAA	Dichloroacetic acid
DCAN	Dichloroacetronitrile
DDA	Dodecylamine
HAAs	Haloacetic acids
HANs	Haloacetronitroles
HKs	Halogenated ketones
HMS	Hexagonal Mesopourous Silicas
HPI	Hydrophilic
HPO	Hydrophobic
MCAN	Monochloroacetronitrile
MPTMS	(3-mercaptopropyl)trimethoxysilane
NOM	Natural organic matter
NR	Natural Rubber
PAC	Powder activated carbon
R^2	Correlation coefficients
TCAN	Trichloroacetronitrile
TCM	Trichloromethane
TEOS	Tetraethyl orthosilicate
THF	Tetrahydrofuran
THMs	Trihalomethanes

LIST OF FIGURES

LIST OF TABLES

CHAPTER I

INTRODUCTION

1.1   STATE OF PROBLEM

Disinfection by-product caused the problem in water such as wastewater or tap water, disinfection of drinking water reduced the microbial risk but increases chemical man risk to human health due to formation of disinfection by-products (DBPs) in the organic and inorganic precursors. The major halogenated DBPs that are identified of chlorination by products are the haloacetic acid (HAAs), haloacetronitriles (HANs), thihalomethane (THMs) and others. There are several techniques that can remove the DBPs from tap water, such as by adsorption (Uyak et al. 2007), ozonation (Vaiopoulou et al. 2015) and membrane filtration (Uyak et al. 2008). Among three processes, the adsorption process has been popular for water treatment because of its advantages that low cost and simple. Although adsorption process has been used in the removal of DBPs on many types of material, there is not having suitable materials for using. Consequently, adsorption process with modified adsorbents would be interesting for removal DBPs from tap water.

Among the porous materials, mesoporous silicas is a number of advantages adsorbent that are widely used in adsorption process because their high surface area and narrow pore size that improve the adsorption capacity and adsorption selectivity. Moreover, hexagonal mesoporous silica (HMS) is the one of many kinds of adsorbent that has been used in the process. In the part, polymer/silica composite has been

studied to make a new material that covers the advantages of silica and organic polymer. Natural rubber (NR) is the organic material that many attempt to modify with material because of its thermal stability and mechanical properties (Nuntang et al. 2014). NR/HMS composite was synthesized and characterized which are attractive for using as adsorbent.

In this study, modification of hexagonal mesoporous silica (HMS) with thiol-group (R-SH) and natural rubber was employed to investigate the effect of surface functional groups on DBPs adsorption capacity comparing with powder activated carbon (PAC) and hexagonal mesoporous silicas (HMS).

The adsorption experiments were carried out by using batch adsorption experiments. The adsorption kinetics and the adsorption isotherm were studied to investigate the adsorption mechanism.

1.2   OBJECTIVES

1.   To investigate adsorption efficiency for disinfection by-product (DBPs) by using thiol-functionalized mesoporous composite based on natural rubber and hexagonal mesoporous silica (NR/HMS-SH).

2.   To investigate the DBPs adsorption selectivity of NR/HMS-SH adsorbent on adsorption of DBPs in tap water.

1.3 HYPOTHESES

1. Hydrophobic surface functional group (Thiol-groups) and natural rubber (NR) can enhance the adsorption capacities of DBPs adsorption.

2. Hydrophobic organic matter in water may be effect the adsorption capacity of DBPs.

1.4 SCOPES OF STUDY

The scope of this research is as follow and the experimental framework is shown in **Figure 1.1.**

1. Four different groups of DBPs, e.g. haroacetronitriles (HANs), haloacetic acids (HAAs), trihalomethans (THMs) and halogenated ketones (HKs) were used as model of DBPs to investigate the adsorption capacity.

2. The adsorption experiments of DBPs on adsorbent were investigated under the batch condition. For adsorption kinetic, the equilibrium time for DBPs was performed by varying the contact time 0 to 36 hours, while the adsorption isotherms were performed by varying concentration of DBPs solution.

3. The organic matters was fractionated into two parts consist of hydrophilic and hydrophobic part.

4. Effects of fractionated organic matter on DBPs adsorption capacities were investigated by conducting adsorption experiment of DBPs in mixed solution.
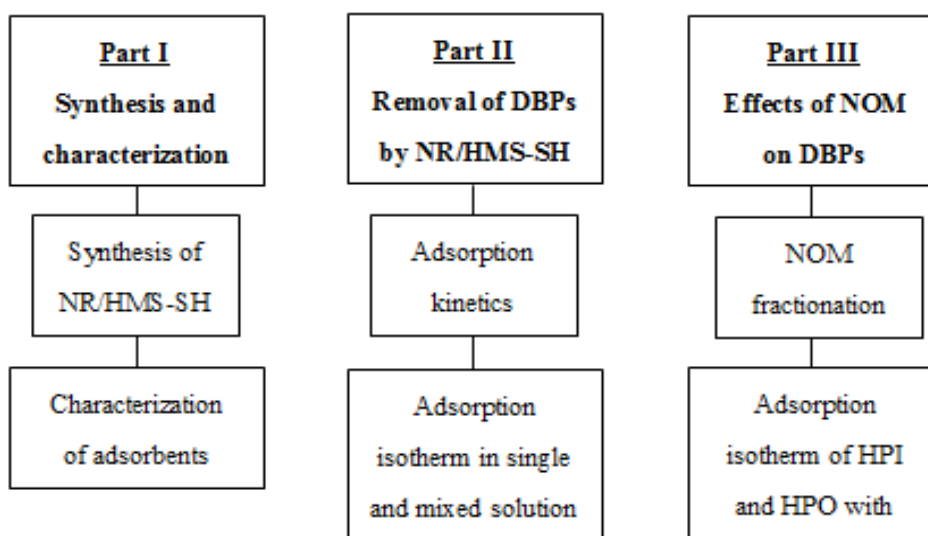
Figure 1.1 Experimental framework of this study
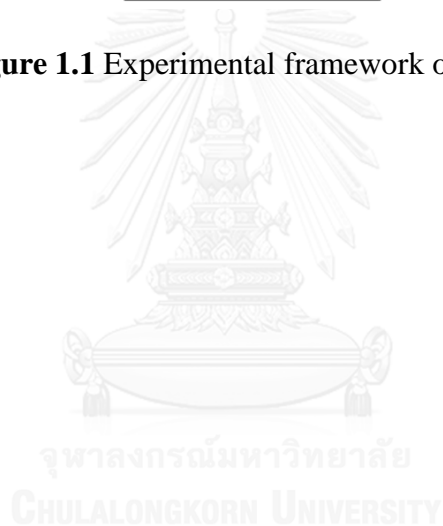
CHAPTER II

THEORETICAL BACKGROUND AND LITERATURE REVIEWS

2.1 THEORY OF ADSORPTION

2.1.1 Adsorption Mechanism

According to adsorption mechanism that is the inter-phase of components in the interfacial layer. It can occur at the interface of two phases of concentration as a driving force. In the solid-liquid adsorption process, three steps are presence in the adsorption process (Albadarin et. al., 2012).

The first step is film diffusion process, which presents the movement of adsorbate molecules to the external surface of the adsorbent. The second step is particle diffusion process that shows the adsorbate molecules move to the interior of adsorpbent particle. The last step is adsorption of the adsorbate onto active sites on the surface of adsorbent. The last step is step that can be negligible because this step is very fast when compared with two steps above. Therefore, the rate limiting step of adsorption process depends on film diffusion or intraparticle diffusion step.

2.1.2 Adsorption Interaction

For solid-liquid adsorption process, there are two kind of surface phenomenon of adsorption include the physical adsorption and chemisorptions.

The physical adsorption includes only weak intermolecule forces such as Electrostratic interaction, hydrogen bonding, hydrophobic bonding and van der Waals

force. The chemisorption involves the formation of a chemical bond between adsorbate and surface of adsorbent. It concerns about the sharing and transfer of electron.

There are many factors that influence the adsorption mechanism on porous materials such as functional groups of adsorbents, polarity, hydrophobicity, molecular weight, dipole moment and aqueous solubility. Moreover, the solution condition (i.e. pH, temperature, concentration, ionic strength and competitive solutes can affect to mechanism of adsorption. In addition, the nature of adsorbents such as surface area, pore size and distribution also made the adsorption mechanism on porous materials changing.

2.1.3 Adsorption Capacity

The adsorption capacity of adsorbent can be determined from mass balance equation as shown in **Equation 2.1.**

$$q = \frac{C_0 - C_e}{M} * V \qquad (2.1)$$

where C_0 and C_e are the initial and equilibrium concentration of the adsorbate (mg/L) respectively, q is the adsorption capacity (mg/g), M is mass of adsorbent (g) and V is volume of solution (L).

2.1.4 Adsorption Kinetic

The objectives of the adsorption kinetic are used to predict and design adsorption systems while chemical kinetic describe rate of chemical reaction. There

are many mathematical models were reported, the pseudo-first-order model and pseudo-second-order model are the generally used to presenting the adsorption behavior.

2.1.2.1 Pseudo-first-order model

Pseudo-first-order model is mostly used procedures for the adsorption of a solute from water solution. Pseudo-first order model can be determined from **Equation 2.2.**

$$\frac{dq_t}{dt} = k_t(q_e - q_t) \qquad (2.2)$$

where q_e is the amount of adsorbed contaminant at equilibrium (mg/g), q_t is the amount of adsorbed contaminant at time (mg/g), and k_1 is rate constant of pseudo-first-order adsorption (h^{-1}).

Integrating Equation 2.2 gets the linear equation and the values of q_e and k_1 are determined from the y intercept and slope of plot, respectively. The non-linear of this model is giving in **Equation 2.3.**

$$q_t = q_e(1 - exp^{(-k_1 t)}) \qquad (2.3)$$

and k_1 value is get from plot of q_t versus t.

2.1.2.2 Pseudo-second-order model

Pseudo-second-order model can be determined from following **Equation 2.4.**

$$\frac{dq_t}{dt} = k_2(q_e - q_t)^2 \qquad (2.4)$$

where k_2 is the rate constant of the pseudo-second-order adsorption (g/mg.hr)

Integrating **Equation 2.4** gets the non-linear form of the pseudo-second-order model as shown in following **Equation 2.5.**

$$\frac{t}{q_t} = \frac{1}{k_2 q_e^2} + \frac{t}{q_e} \qquad (2.5)$$

The initial adsorption rate can be determined in **Equation 2.6.**

$$h = k_2 q_e^2 \qquad (2.6)$$

where *h* is initial sorption rate.

2.1.2.3 Intraparticle diffusion model

In 1962, Weber and Morris had presented the intraparticle diffusion model that used to predict the rate of controlling step in the adsorption process. (Weber & Morris 1962). The intraparticle diffusion can be determined as **Equation 2.7.**

$$q_t = k_i t^{\frac{1}{2}} + C \qquad (2.7)$$

Where q_t is the amount of adsorbate adsorbed (mg/g) at time $t^{1/2}$ (min$^{1/2}$), k_i is the intraparticle diffusion rate constant (mg/g.min$^{1/2}$) and C is the interception. It can be determined from the plot of q_t vs $t^{1/2}$.

2.1.5   Mass transfer

Mass transfer parameter (k_f , k_s , K_s , K_f and D_s) was calculated by using the adsorption kinetic and isotherm data. Mass transfer through liquid film can write in rate law that calls "Linear driving force" (LDF) was investigated and calculated as shown **Equation 2.8.**

$$\frac{\partial \overline{q}}{\partial t} = k_f S_0 (C - C_i) \qquad (2.8)$$

$\overline{q}$ is the average solute concentration in solid (M/V). C is the concentration of the solute in bulk solution (M/V). C_i is the concentration of solute in liquid interface (M/V). S_0 is the surface area of particle per unit volume of adsorbent (M/V) and k_f is the liquid film mass transfer coefficient (L/T).

Mass transfer through particle pore can describe by "Homogeneous solid diffusion model" (HSDM) that has Diffusivity (D_s) as shown in **Equation 2.9.**

$$\frac{\overline{q}}{q_\infty} = 6 \left(\frac{D_s t}{R^2} \right)^{1/2} \left[\pi^{1/2} + L \right] \qquad (2.9)$$

r is the radial position (L) and D_s is constant diffusivity (L^2/T). D_s can calculate from the slope value and q_∞ is average solute concentration in solid at infinite time.

Mass transfer through solid film in rate law calls "Linear driving force (LDF) that shown in **Equation 2.10.**

$$\frac{\partial \overline{q}}{\partial t} = k_s S_0 (q_i - \overline{q}) \qquad (2.10)$$

q_i is the solid concentration at interface (M/V) and k_s is the solid film mass transfer coefficient (L/T).

The presence of Overall solid-phase mass transfer coefficient (K_s) can be rewritten as **Equation 2.11.**

$$\frac{\partial \overline{q}}{\partial t} = K_s S_0 (q_e - \overline{q}) \qquad (2.11)$$

K_s is Overall solid-phase mass transfer coefficient and q_e is value of q at equilibrium (M/V).

$$\frac{1}{K_s} = \frac{m}{k_f} + \frac{1}{mk_s} \qquad (2.12)$$

m is slope of a plot between q and C.

In case of the presence of Overall liquid-phase mass transfer coefficient (K_f) can be rewritten as **Equation 2.13.**

$$\frac{\partial \overline{q}}{\partial t} = K_f S_0 (C - C_e) \qquad (2.13)$$

C_e is value of C at equilibrium (M/V).

$$\frac{1}{K_f} = \frac{1}{k_f} + \frac{1}{mk_s} \qquad (2.18)$$

According to Equation 16 and 18, it has relationship between K_s and K_f as **Equation 2.14.**

$$K_f = mK_s \qquad (2.14)$$

2.1.6   Adsorption Isotherm

For adsorption isotherms, the equilibrium adsorption capacity (q_e) and the final equilibrium concentration (C_e) are plotted to study the relationship. The equilibrium adsorption capacity (q_e) can be calculated from the **Equation 2.15.**

$$q_e = \frac{(C_0 - C_e)V}{M} \qquad (2.15)$$

where C_0 is the initial concentration (mg/L), C_e is the equilibrium concentration (μg/L), V is the volume of the solution (L), and M is the mass of adsorbent (g). The adsorption isotherm relationship can be mathematically expressed by many models.

Linear, Langmuir and Freundlich models are used for explain the adsorption isotherm of DBPs removal.

2.1.3.1 Linear Model

Linear model is simple isotherm. The linear isotherm shows relationship between concentration of adsorbate and the amount of adsorbate that adsorbed at the equilibrium. This isotherm can be shown in the following **Equation 2.16.**

$$q_e = K_p C_e \qquad \qquad \textbf{(2.16)}$$

where q_e is the amount of adsorbate that adsorbed at the equilibrium (mg/g), K_p is linear constant (L/mg), and C_e is concentration of adsorbate at equilibrium (mg/L).

2.1.3.2 Langmuir isotherm

The Langmuir sorption isotherm (Langmuir, 1916) was proposed to one of adsorption isotherm. The Langmuir isotherm of linear form can be written in the **Equation 2.17.**

$$\frac{1}{q_e} = \frac{1}{K_L q_m C_e} + \frac{1}{q_m} \qquad \qquad \textbf{(2.17)}$$

where q_e is the amount of adsorbate that adsorbed at the equilibrium (mg/L), q_m is the maximum adsorption capacity (mg/g), K_L is the Langmuir constant (L/mg).

2.1.3.3 Freundlich isotherm

Freundlich model is an empirical equation that describes the adsorption process based on the assumption. The Freundlich isotherm does not predict any

saturation of the sorbent by the sorbate. This isotherm can be written as **Equation 2.18.**

$$q_e = K_F C_e^{\,1/n} \tag{2.18}$$

where K_F and n are constants, and C_e is the equilibrium concentration (mg /L). This equation can be written in linear form as shown in **Equation 2.19.**

$$\ln(q_e) = \ln(K_F) + \frac{1}{n}\ln(C_e) \tag{2.19}$$

where K_F is Freundlich constant and n is adsorption intensity (dimensionless). Moreover, the value of K_F and n depend on temperature, the nature of adsorbent and the adsorbate property.

2.2   ADSORBENTS

2.2.1   Mesoporous silica

Mesoporous silicates are one in three classes of porous material. These materials are important to use as an adsorbent because their characteristics that are large surface area, high mesopore volume, and narrow pore size distribution. Consequently, they are suitable for many applications such as catalysis, separation, and adsorption process.

In 1992, Mobil scientists found mesoporous silicas (Tanev & Chibwe, 1994), that materials have widely used in separation, catalysis and adsorption due to their various advantages such as high surface area, large surface area and large uniform pore size and large pore volume which can improve the adsorption capacity and the selective adsorption.

In 1949, Dickey revealed that sol-gel process to synthesize silica based adsorbent. Pore size and shape of the inorganic porous materials can control by molecular imprinting (Dickey, 1949).

2.2.2 Hexagonal mesoporous silica

Hexagonal mesoporous silica (HMS) is a kind of mesoporous silica produced by the neutral synthesis pathway. HMS was synthesized in the present of neutral inorganic precursors and uncharged surfactants.

2.2.3 Adsorbent surface modifications

There are two general methods to modify surface characteristics of siliceous mesoporous materials which are co-condensation method and post-grafting method.

2.2.3.1 Co-condensation method

This method is a one-step procedure between silica precursors with organosilane and allows better control of loading and distribution of organo-functional groups, but it produces less order mesoporous structure.

2.2.3.2 Post grafting method

Post grafting is the method of the surface via the reaction of silanol groups with organosilane. It can be used to prepared well order functionalized mesoporous material.

2.3   NATURAL ORGANIG MATTER (NOM)

Natural organic matter (NOM) is the group of organic material that presented in surface water or ground water. Humic and non-humic fractions are the part of NOM. The dissolved fraction of NOM may not be fully removed using conventional water treatment practices and have been shown to produce by-products such as trihalomethanes (THMs) during disinfection. NOM composed with aromatic, aliphatic, quinonic and phenolic structure with several molecule size and their properties. It can separate into two fractions that hydrophobic (HPO) and hydrophilic (HPI) NOM. Hydrophobic NOM consist poly-aromatic carbon, phenolic and conjugated double bond in the molecules whereas hydrophilic NOM consist higher aliphatic carbon and nitrogenous compound.

2.4   DISINFECTION BY-PRODUCTS
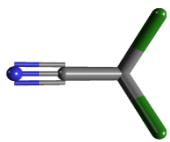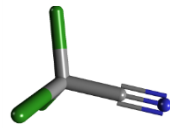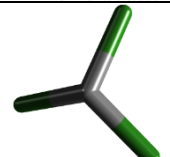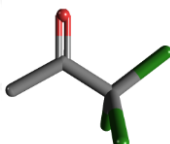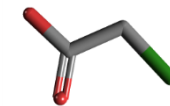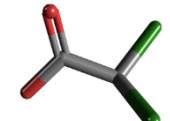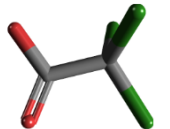
Disinfection by-products (DBPs) are reaction between several organic and inorganic compound in water that formed by aqueous free chlorine and natural organic matter (NOM). There are many DBPs that present in water such as halogeneted DBPs such as trihalomethane (THMs), haloacetic acids (HAAs), haloacetronitriles (HANs) and haloketones (HKs).

Many of DBPs are present in low concentration, while exposure at low levels of DBPs revealed for over long periods of time. These affected to human health when the people use the water for drinking, washing or cooking. The United States Environmental Protection Agency (USEPA) has set Maximum Contaminant Levels (MCLs) for haloacetic acids (HAAs) and total trihalomethanes (THMs). In Europe,

the level of THMs has been set at 0.1 mg/L under the Drinking Water Directive. No guideline values have been set for HAAs in Europe. The World Health Organization has established guidelines for several DBPs such as chloroform, dichloroacetic acid, dichloroacetonitrile (DCAN) and trichloroacetic acid (TCAA). The physico-chemical properties of DBPs are summarized in **Table 2.1**.

Table 2.1 The physico-chemical properties of disinfection by-products (DBPs)

Name of DBPs	Molecular structure	Molecular weight (g/mol)	Water solubility (mg/mL)	pK$_a$	Boiling point (°C)
Monochloroacetonitrile (MCAN), CH$_2$ClCN		75.50	100	-	126
Dichloroacetonitrile (DCAN), CHCl$_2$CN		109.94	10-50	-	112
Trichloroacetonitrile (TCAN), CCl$_3$CN		144.39	<1	-	181
Trichloromethane (TCM), CHCl$_3$		119.38	8.0	-	61.2
1,1,1-Trichloroacetone (C$_3$H$_3$Cl$_3$O)		161.42	7.45	-	135
Monochloroacetic acid (MCAA), CH$_2$ClCOOH		94.49	858	2.87	189
Dichloroacetic acid (DCAA), CHCl$_2$COOH		128.90	miscible	1.35	194
Trichloroacetic acid (TCAA), CCl$_3$COOH		163.38	1.45	0.77	196

2.5 LITERATURE REVIEWS

2.5.1 Natural rubber and hexagonal mesoporous silica

In the past decade, natural rubber (NR) was attempted to modify the properties through many techniques, such as functionalization (Okwu and Okieimen 2001), hydrogenation (Pruttisirikula, et. al. 2010) and adding nanofillers. In the nanofillers technique, researchers interested in the incorporation of silica fillers in the rubber polymer due to it useful properties. The interesting resultant particle filled composites given the increased thermal stability and mechanical properties.

In 2014, the novel composite material with a high mesoporosity based on natural rubber (NR) and hexagonal mesoporous silicas (HMS) was synthesized via in situ sol-gel process and characterized. The incorporation of natural rubber (NR) molecules in the mesoporous structure enlarged the unit cell and channel wall thickness of hexagonal. The NR/HMS composites represented the high BET surface area, large pore volume and narrow pore size distribution. The composites revealed a highly ordered hexagonal meso-structure which enhanced textural properties and hydrophobicity. Therefore, they are attractive for using as adsorbents and catalyst supports (Nuntang, et. al. 2014)

2.5.2 Removal of disinfection by-products

In the previous study, many researchers concentrated on disinfection by-products (DBPs) that can cause many effects for a long exposure. The most DBPs that were interested and caused risk are chlorination DBPs. Some species of these DBPs

lead to health effect include cancer and reproductive defects (United States Environmental Protection Agency, 1998 and United States Environmental Protection Agency, 2003). The United States Environmental Protection Agency (2003) represented the maximum levels for trihalomethanes (THMs) and haloacetic acids (HAAs), two of the most prevalent DBPs.

There are many processes such as adsorption (Uyak, Yavuz et al. 2007), (Prarat et al. 2011), ozonation (Vaiopoulou, Misiti et al. 2015) and membrane filtration (Uyak, Koyuncu et al. 2008), which can remove the disinfection by-product (DBPs) from the water.

There have advantages and disadvantages in each process; adsorption process has been popular for DBPs removal due to its advantages that low cost and simple. Many researches have been done on adsorption process of DBPs removal that using porous materials (Babi et al. 2007) (Kim and Kang 2008) and many studies have been investigated carbon adsorption. (Tung et al. 2006) studied the adsorption characteristics of HAAs on GAC. They found that HAAs had lower adsorption capacity than THMs because may be able to biodegradation. Because of biodegradation, (Ratasuk et al. 2008) found that biological activated carbon is more efficient for HAAs removal.

2.5.3   Adsorption of DBPs by porous materials

From the previously reviews, adsorption process by activated carbon is suitable for some group of DBPs removal. Therefore the development adsorbents are interesting for study. Among the porous materials, mesoporous silicates is a number

of advantages as adsorbents because of their high surface area, large pore volume and narrow pore size distribution. Hexagonal mesoporous silicates (HMSs) with pure silica framework and different functionalized surfaces had shown to be effective adsorbents for DCAA removal and the properties of DCAA with the amino functionalized is excellent (Punyapalakul and Takizawa 2006). (Prarat, Ngamcharussrivichai et al. 2011) studied the adsorption of HANs by mesoporous materials in aqueous solution. They found that the adsorption rate and capacity of HANs both significantly influenced by different porous and crystalline structures. Mercapto-functionalized HMS (M-HMS) provided higher adsorption capacity of HANs than the other organic-functionalized adsorbents and the different molecular structure of HANs affected the adsorption capacity and selectivity over M-HMS. In addition, the effect of electrolyte in tap water and the presence of co-existing DBPs (trihalomethanes and haloacetic acid) did not affect to the selective adsorption of adsorbent.

2.5.4 Effect of NOM on adsorption capacity

In the previous study about effect of natural organic matter (NOM), there are various research that studied effect of NOM by using powdered activated carbon (PAC) in batch adsorption experiments to remove trace synthetic organic chemicals (SOCs) from water containing natural organic matter (NOM) (Matsui et. al. 2003). The percentage of SOC removal at various contact time and the weight of PAC did not depend on initial SOC concentration. The percentage of SOC removal for the strongly adsorbing SOCs did not depended on only at low concentrations. The

fractionation of NOM competed with the weakly SOC that showed a higher percentage of the total NOM than compete with the strongly SOC. The adsorption capacities of the SOC represented the perfectly reduced in the water that NOM containing.

Moreover, in 2005 there is some study about adsorption capacities for atrazine on granular activated carbon (GAC) in batch experiments. The results showed the adsorption capacity of atrazine that competed with dissolved organic carbon (DOC). The adsorption capacities were generally greater than 10 mg/g. Moreover, the results indicated that DOC competition decreased the atrazine adsorption capacities (Wang 2005).
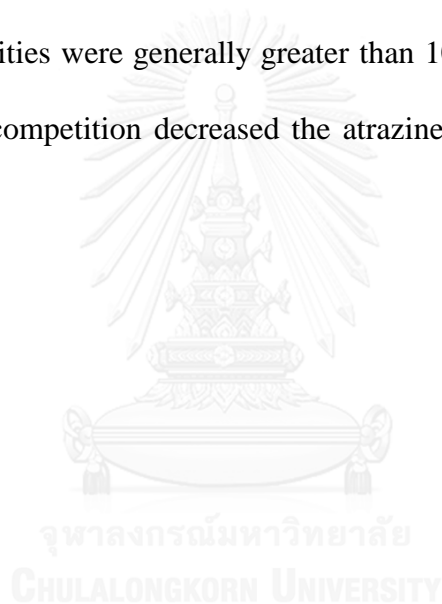
CHAPTER III

MATERIALS AND METHODS

3.1   MATERIALS

3.1.1   Chemical Reagents

- Chloroacetic acid	99%	SIGMA-ALDRICH
- Chloroacetonitrile		Wako
- Copper (II) sulphate		CARLO ERBA
- Calcium chloride		UNIVAR
- Dichloroacetonitrile	98%	SIGMA-ALDRICH
- Dichloroacetic acid	99%	ACROS ORGANICS
- Dipotassium hydrogen phosphate	99%	CARLO ERBA
- Dodecylamine	98%	SIGMA-ALDRICH
- Ethanol	99.9%	QRëC
- Ethyl alcohol absolute		Fisher Scientific UK
- Hydrochloric acid	37%	QRëC
- Methanol	HPLC	Fisher Scientific UK
- Methyl-tert butyl ether	HPLC	Fisher Scientific UK
- Natural Rubber	Thai Hua Chumporn Natural Rubber Co., Ltd. (Thailand)	
- Potassium hydrogen phosphate		QRëC
- Sodium chloride		CARLO ERBA
- Sodium hydroxide		CARLO ERBA
- Sodium hydrogen carbonate		QRëC

- Sodium sulphate	99%	CARLO ERBA
- Sulfuric Acid	98%	QRëC
- Tetraethyl orthosilicate	98%	SIGMA-ALDRICH
- Trichloroacetic acid	≥99%	SIGMA-ALDRICH
- Trichloromethane		Fisher Scientific UK
- Tetrahydrofuran	99.5%	QRëC
- Trichloroacetronitrile	98%	SIGMA-ALDRICH
- 1,1,1-Trichloroacetone	>95%	TCI
- 2,3-dibromopropionic acid		Fluka
- (3-mercaptopropyl)trimethoxysilane	95%	SIGMA-ALDRICH

3.1.2   Laboratory Equipment

- Elemental Analyzer (EA) (CHNS/O Analyzer)

- Fourier Transform Infrared Spectrometer (FTIR)

- Gas Chromatrography (GC)

- High Performance Liquid Chromatrography (HPLC)

- Magnetic stirrer

- pH meter

- Scanning Electron Microscope (SEM)

- Syringe filter (Nylon, 0.45 μm)

- Thermometer

- Total Organic Carbon analyzer (TOC)

- UV/ visible spectrophotometer

- Vacuum pump

- VF-X Varian Column (30 m x 0.32 mm)

- X-Ray Diffractrometer (XRD)

3.2   METHODOLOGY

3.2.1   Part I: Synthesis and characterization of NR/HMS-SH.

3.2.1.1 Preparation of adsorbent

Synthesis of thiol-functionalized mesoporous composite based on natural rubber and hexagonal mesoporous silicate (NR/HMS-SH) according to condition of NR/HMS-SO$_3$H synthesis by (Nuntang, Poompradub et al. 2014). Firstly, 1 g of natural rubber (NR) sheet was mixed with 30 mL of tetrahydrofuran (THF) at room temperature for 3 h to overnight which the NR sheet dissolved in THF to obtain a homogeneous solution. Secondly, 7.51 g of dodecylamine (DDA) was added in the solution and stirred. After 0.5 h, 21 g of tetraethylorthosilicate (TEOS) was added and stirred for 0.5 h too. Next, 106 g of H$_2$O was added and stirred at 40 ^{o}C for 0.5 h and then 3-mercaptopropyltrimethoxysilane (MPTMS) was added into mixture with stirring to stand at 40 ^{o}C for 1 h. The gel was at 40 ^{o}C for 3 days after which it was precipitated in 100 mL of ethanol. The solid product was vacuum dried at 60 ^{o}C for 2 h. Finally, the template in composite was removed with 0.05 M of H$_2$SO$_4$/EtOH at 70 ^{o}C for 8 h and filtered; vacuum dried with ethanol, check pH around 7 and dried at 80 ^{o}C for overnight.

3.2.1.2 Characterization of NR/HMS-SH

Porous structure

Silica structure analysis of adsorbents was measured by Low-angle Powder X-ray diffraction (XRD) equipped with Cu Kα radiation. The XRD patterns were collected in scanning rate 1000 deg/min from 0.5° to 6.0° (2θ).

Surface area and Pore size

Surface area, pore volume and pore diameter were determined by nitrogen adsorption-desorption isotherms at 77 °K using an Autosorb-1 Quantachrome automatic volumetric sorption analyzer. Adsorbents were heated at 105 °C for 2 hr before analysis. After that, the specific surface area (S_{BET}) was calculated by using Brunner-Eller-Teller (BET) equation while pore diameter and pore volume (V_p) was calculated by using Barrett-Joyner-Halenda (BJH) equation.

Surface functional groups

Surface functional groups were analyzed by Fourier-Transform Infrared Spectrometer (FTIR). Before measurement, the adsorbent powder was heated at 105 °C in the oven for 2 hr and kept in desiccators until analysis. The adsorbent powder was mixed with KBr and FTIR spectra were recorded in the transmittance mode from 400 – 4000 cm^{-1}.

Elemental analysis

The amount of sulfur of mercapto-functionalized on adsorbent (NR/HMS-SH) was measure by using CHONS analyzer. Coal reference material was used a sulfur standard. The % (w/w) of sulfur was calculated by comparing with sulfur in coal reference.

Scanning Electron Microscope (SEM)

The particle size of the adsorbents was measured by scanning electron microscope (SEM). Before measurement, all samples were fixed on aluminum stubs and coated.

Surface charge measurement

Surface charge density of adsorbents was measured by acid-base titration method. HCl and NaOH stock solutions were prepared at 25 mM. 0.025 g adsorbent was mixed in difference volume of HCl and NaOH stock solutions in order to vary the pH of solution. The ionic strength (IS) was fixed at 10 mM by adding 2.5 mL of 0.1 M NaCl solution. The final volume is 25 mL. Then the samples were stirred in 125 mL Erlenmeyer flask at 25 ^{o}C. After 12 hr, the pH of solution was measured by using pH meter and calculated the surface charge density following the **Equation 3.1**

$$\boldsymbol{Surface\ charge}\ (\boldsymbol{Cm^{-2}}) = \frac{\{[HCl] - [NaOH] - [H^+] + [OH^-]\}}{M\ x\ S_{BET}}\ \boldsymbol{x\ 96,500} \qquad (3.1)$$

where [HCl], [NaOH] are concentration (M) of HCl and NaOH, respectively. [H$^+$] is the concentration of hydrogen ion (M) as calculated from pH = -log [H$^+$], [OH$^-$] is the concentration of hydroxide ion (M) as calculated from pOH = -log [OH$^-$] and pOH = 14 − pH, 96,500 is Faraday constant (Coulomb mol^{-1}), M is mass of adsorbent (g/L) and S_{BET} is specific area of adsorbents (m^2/g).

Table 3.2   Characterization of NR/HMS-SH

Parameter	Measurement
Silica porous structures	X-ray diffractometer (XRD)
Surface area and pore size	N$_2$ adsorption-desorption isotherms
The presence of surface functional groups	Fourier-Transform Infrared Spectrometer (FTIR)
Amount of Sulfur	Elemental Analyzer
Particle size	Scanning Electron Microscope (SEM)

3.2.2   Part II: Removal of DBPs by NR/HMS-SH.

3.2.2.1 Preparation of stock solution

Stock solutions of disinfection-by products (DBPs) were prepared in deionized water that pH of solution and 10 mM of ionic strength (IS) was adjusted by using phosphate buffer.

3.2.2.2 Adsorption experiments

Adsorption kinetic study

The kinetic study was prepared by varying contact time from 0 to 36 h. DCAN was selected as a model of HANs; DCAA was selected as a model of HAAs; trichloromethane (TCM) was selected as a model of THMs and 1,1,1-Trichloroacetone ($C_3H_3Cl_3O$) was selected as a model of HKs for batch adsorption kinetic. The initial DCAN, TCM and $C_3H_3Cl_3O$ concentration for NR/HMS-SH was 1 mg/L and PAC was 0.5 mg/L at pH 7. The initial DCAA concentration for NR/HMS-SH and PAC was 0.5 mg/L at pH 7, while the ionic strength remain fixed at 10 mM adjusted by a phosphate buffer. The mixture was stirred in 125 mL Erlenmeyer flask at 25 ^{o}C and the supernatant solution was filtrated through a nylon syringe filter (pore size 0.45 mm). The concentration of DCAN, TCM and $C_3H_3Cl_3O$ was analyzed by a gas chromatograph equipped with electron capture detector (GC/μECD) according to the EPA method 551.1 and DCAA concentration was determined following by EPA method 552.2.

Adsorption isotherm study

Adsorption isotherm was conducted with the initial concentration of each HAAs (such as DCAA), HANs (MCAN, DCAN and TCAN), TCM and $C_3H_3Cl_3O$ for NR/HMS-SH and PAC was varied from 0.05 to 2 mg/L in single solution at pH 7, while the ionic strength remain fixed at 10 mM adjusted by a phosphate buffer. The contact time was received from kinetic studies. The mixture was stirred in 125 mL Erlenmeyer flask at 25 ^{o}C. After equilibrium, the supernatant solution was filtrated

through a nylon syringe filter (pore size 0.45 mm). The concentration of HANs, TCM and $C_3H_3Cl_3O$ was analyzed by GC/µECD according to the EPA method 551.1 and HAAs concentration was determined following by EPA method 552.2.

Selective adsorption study

The selective adsorption of adsorbents in the presence of DBPs on NR/HMS-SH and PAC was performed by mixing the four DBPs species, e.g. dichloroacetic acid (DCAA), dichloroacetronitrile (DCAN), trichloromethane (TCM) and 1,1,1-Trichloroacetone ($C_3H_3Cl_3O$), at the same concentration at pH 7 with ionic strength of 10 mM. The initial concentration of the four DBPs was varied from 0.05 to 1 mg/L. The mixture was stirred in 125 mL Erlenmeyer flask at 25 °C. After equilibrium, the supernatant solution was filtrated through a nylon syringe filter (pore size 0.45 mm). The concentration of DCAN, TCM and $C_3H_3Cl_3O$ was analyzed by a gas chromatograph equipped with electron capture detector (GC/µECD) according to the EPA method 551.1 and DCAA concentration was determined following by EPA method 552.2.

3.2.2.3 Analytical Methods

Determination of Haloacetronitriles (HANs), Trichloromethane (TCM) and 1,1,1-Trichloroacetone ($C_3H_3Cl_3O$)

Haloacetronitriles (HANs), Trichloromethane (TCM) and 1,1,1-Trichloroacetone ($C_3H_3Cl_3O$) was analyzed following by modified EPA Method 551.1. A 25 mL sample solution was filled in 40 mL glass vial with cap and faced

septum. Then, 5 g of sodium sulphate anhydrous (Na_2SO_4) and 2 mL of methyl *tert*-butyl ether (MTBE) was added in each sample. Each sample was shaken for 2 min and standing the solution for 3 min. After that 500 μL of the MTBE layer was transferred to GC vial and analyzed by gas chromatography with an electron capture detector (GC/μECD).

Determination of Haloacetic acids (HAAs)

Haloacetic acid (HAAs) was analyzed following by modified EPA Method 552.2. In derivatization step, a 15 mL sample solution was filled in 40 mL glass vial with cap and faced septum. Then, the 25 μL of 30 ppm surrogate standard and 0.5 mL of concentrated sulfuric acid (H_2SO_4) were added, respectively. After that, 4 g of Na_2SO_4 was added and shaken until dissolved. The sample was quickly added with 1.5 g of copper sulphate pentahydrate ($CuSO_4.5H_2O$) and 2.5 mL of MTBE. Each sample was shaken for 2 min and standing the solution for 3 min.

In methylation step, A 1,625 μL 0f MTBE layer was transferred to 40 mL glass vial with cap and faced septum. A 2 mL of 10% H_2SO_4 in methanol was added into the sample and the vial was placed in a water bath at $50^{o}C$ for 2 h. then, it was cooled at $4^{o}C$ for 2 min and then 5 mL of saturated sodium bicarbonate ($NaHCO_3$) was added. The vial was shaken for 2 min to release carbon dioxide (CO_2) and was stood for 5 min. The 500 μL of the MTBE layer was transferred to GC vial and analyzed by gas chromatography with an electron capture detector (GC/μECD).

3.2.3   Part III: Effects of NOM on DBPs adsorption capacity.

3.2.3.1 NOM fractionation

First, water sample was adjusted pH to 2 by using by H_2SO_4 and passed through the columns which containing DAX-8 resin with a flow rate of less than 0.33 mL/sec. The effluent water from DAX-8 resin column was contained the hydrophilic (HPI) fraction. While the hydrophobic (HPO) fraction was adsorbed on the DAX-8 resin which can be eluted from resin by using 0.1 M of NaOH, 50 mL and 0.01 M of NaOH, 250 mL, respectively. Fractionated samples of each fraction was adjusted pH to 7 and filtrated with 0.45 μm GF/C filter paper before analyzed for their organic fractions (Rakruam and Wattanachira 2014).

3.2.3.2 NOM concentration measurement

The concentration of NOM in tap water sample was analyzed by using dissolve organic carbon measurement (TOC) and UV/ visible spectrophotometer (230 nm).

3.2.3.3 Adsorption experiments

Fractionated NOM was added in to the solution as prepared by the method described in adsorption isotherm experiment. The obtained adsorption isotherms and mixed system was compared to the isotherms in single solute in order to investigate the effect of NOM on DBPs adsorption capacity. Adsorption isotherm was conducted with the initial concentration of DCAN from 0.1 to 1 mg/L. The mixture was stirred

in 125 mL Erlenmeyer flask at 25 ^{o}C. After equilibrium, the supernatant solution was filtrated through a nylon syringe filter (pore size 0.45 mm). Then, the remaining NOM and DCAN concentration was analyzed by UV/ visible spectrophotometer (230 nm) and GC/μECD, respectively.

CHAPTER IV

RESULTS AND DISCUSSION

4.1   CHARACTERIZATION

Synthesized adsorbents were characterized physio-chemical properties by various instruments such as X-ray diffraction (XRD), N_2 adsorption-desorption isotherms, Fourier Transforms Infrared Spectroscopy (FTIR), CHONS Elemental analyzer, surface charge density and particle size. Obtained data was use to evaluated the DBPs adsorption capacity and mechanism by NR/HMS-SH.

4.1.1   X-ray Diffraction (XRD)

X-ray diffraction (XRD) was used to evaluate crystalline structure and analyze the structure of NR/HMS-SH at 2θ angle of 0.5°-10.0° as shown in **Figure 4.1**. The XRD patterns of NR/HMS-SH showed at 2θ = 2.5° that referred to the hexagonal mesoporous silica structure of NR/HMS-SH as reported by Nuntang et al. that the 2θ value of HMS compound and NR/HMS composite in the wall thickness and expanse of unit cell of HMS that can decrease intensity of 2θ value (Nuntang,et. al. 2014). The result suggested that the NR molecules were incorporated unto the hexagonal mesoporous structure of HMS.
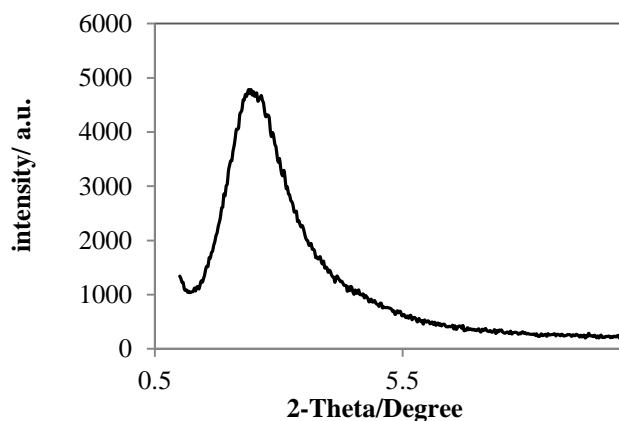
Figure 4.1 XRD pattern of NR/HMS-SH

4.1.2 N_2 adsorption-desorption isotherms

Surface area, pore volume and pore diameter of all adsorbents were characterized by using N_2 adsorption-desorption isotherms as shown in **Figure 4.2.**
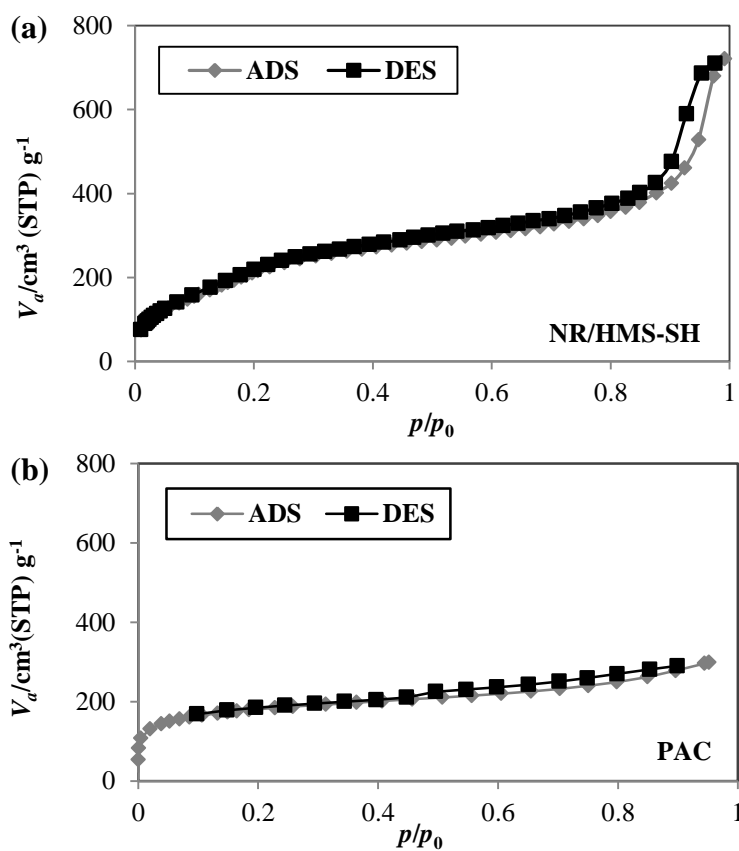
Figure 4.2 N_2 adsorption-desorption isotherms of (a) NR/HMS-SH and (b) PAC.

The surface area was calculated by Brunauer-Emmett-Teller (BET) equation, while the pore volume and pore diameter of adsorbents were calculated using Barrett-Joyner-Halenda (BJH) equation. According to IUPAC classification, type IV isotherm was used to determine the mesoporous structure of NR/HMS-SH. The NR/HMS-SH composites possessed a high BET surface area, small pore size and large pore volume. Moreover, PAC represented type I isotherm which indicates the presence of micropores. Calculated porous information such as pore diameter, pore volume (Vp) and surface area was concluded in **Table 4.1**.

Table 4.1 Mean pore diameter, pore volume, and BET surface area of NR/HMS-SH and PAC.

Adsorbents	Functional group	Mean pore diameter (nm)	V_P ($cm^3 g^{-1}$)	S_{BET} ($m^2 g^{-1}$)
NR/HMS-SH	Silanol and thiol groups	2.534	1.116	880.4
PAC	Carboxyl, phynyl and oxygen-containing groups	2.858	0.4627	647.5

4.1.3   Fourier Transforms Infrared Spectroscopy (FTIR)

The functional groups presenting on the surface of adsorbent were identified by using FTIR spectroscopy as shown in **Figure 4.3.**

The O-H stretching of silanol groups was observed at 3450 cm^{-1} and the Si-O stretching was detected around 1100 cm^{-1}. C-H stretching of NR structure was observed in 2920 cm^{-1}. The presence of thiol-group should have the peak of S-H stretching at 2490-2580 cm^{-1} but the peaks cannot show in these spectra. It might be difficult to identify peaks of thiol group and it might be interfere by other functional

groups. However, the thiol group can confirm by CHONS analyzer in next measurement.
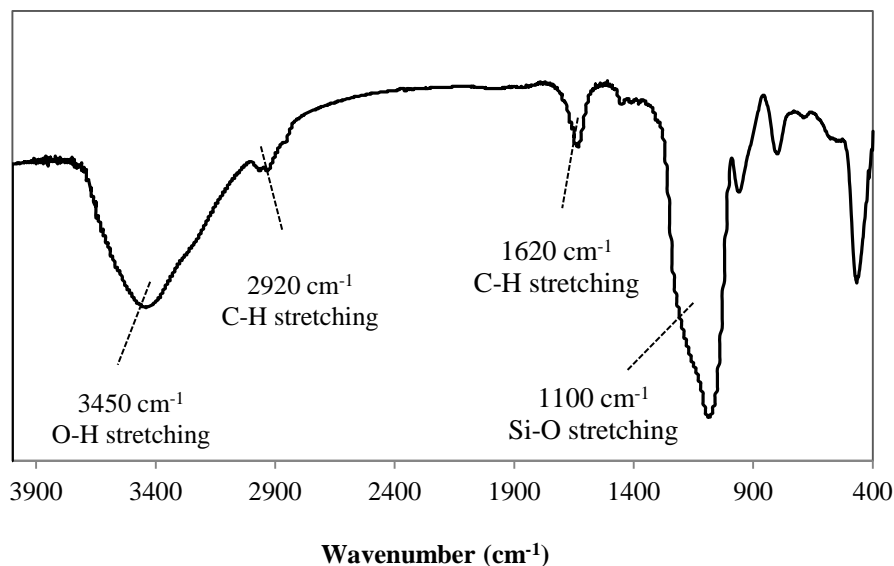
Figure 4.3 FTIR spectrum of NR/HMS-SH

4.1.4 CHONS Elemental Analysis

The sulfur analyzer technique was applied for sulfur quantification. The sulfur content of NR/HMS-SH was 5.670 % w/w, confirming the presence of thiol-group (-SH) on the surface of NR/HMS-SH as shown in **Table 4.2.**

Table 4.2 Content of total Sulfur (% w/w) of NR/HMS-SH

Adsorbents	% Carbon	% Hydrogen	% Nitrogen	% Sulfur
NR/HMS-SH	21.47	3.600	0.000	5.670

4.1.5   Surface Charge Density

The surface charges density (Coulombs m^{-2}) of the NR/HMS-SH and PAC was measured by acid-base titration technique and calculated following **Equation 3.1** (see in Chapter 3). After calculating, the surface charges density (Coulombs m^{-2}) of adsorbents versus pH of solutions was plotted in the **Figure 4.4.** It can conclude that the surface charge density decreases while increasing the pH from acidic to basic. The surface site of NR/HMS-SH was protonated bring about to the positive charge of surface at low pH. In the same time, at high pH the surface hydroxides eradicated proton lead to negative charge surface. Moreover, the pH$_{PZC}$ of NR/HMS-SH and PAC were 5.46 and 6.92, respectively.
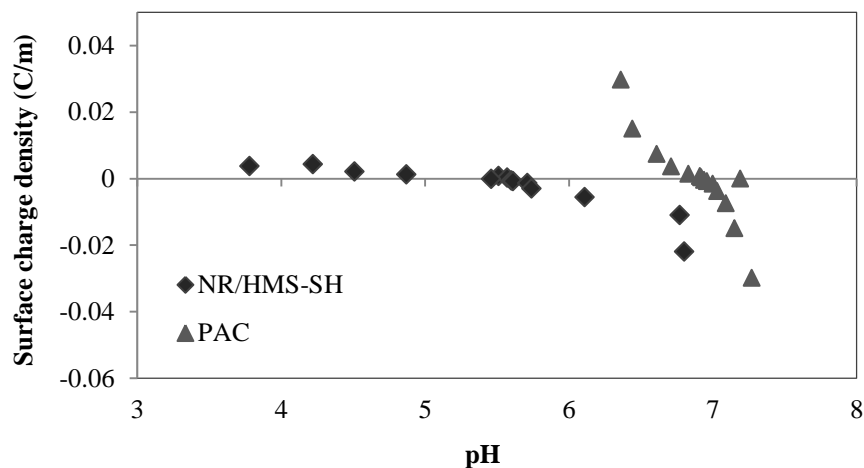
Figure 4.4 Surface charges of NR/HMS-SH and PAC as a function of pH solution

4.1.6   Particle size distribution analysis

The particle size distribution was analyzed by scanning electron microscope (SEM) and the image of NR/HMS-SH is shown in **Figure 4.5.** The images of

NR/HMS-SH exhibited small spherical aggregates of silica particles that were homogeneously dispersed in the agglomerates.
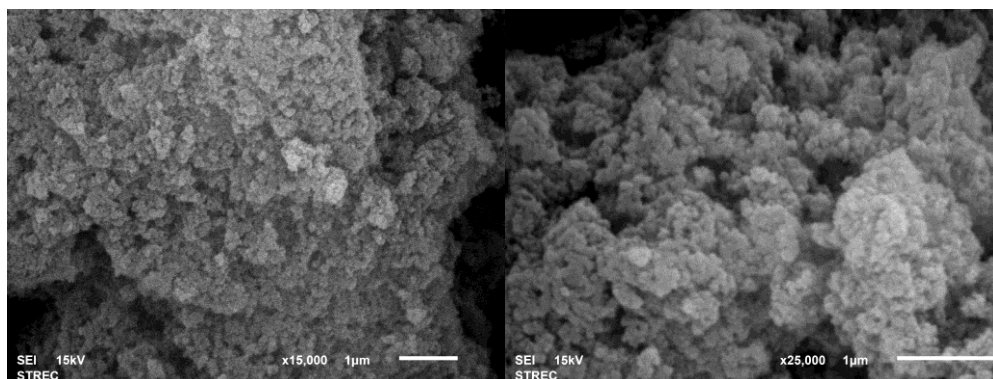
Figure 4.5 Representative SEM images of NR/HMS-SH

4.2   ADSORPTION OF NR/HMS-SH

4.2.1   Adsorption kinetic

The kinetic study of NR/HMS-SH and PAC was prepared by varying contact time from 0 to 36 h. The initial DCAN, TCM and $C_3H_3Cl_3O$ concentration for NR/HMS-SH was 1 mg/L and PAC was 0.5 mg/L at pH 7. The initial DCAA concentration for NR/HMS-SH and PAC was 0.5 mg/L at pH 7, while the ionic strength remain fixed at 10 mM adjusted by a phosphate buffer.

Kinetic curve of DBPs adsorption including TCM, $C_3H_3Cl_3O$, DCAN and DCAA on synthesized porous adsorbents are (NR/HMS-SH and PAC) are shown in **Figure 4.6.** The results showed that the DCAN concentration of NR/HMS-SH reach equilibrium at 12 h. Interestingly, the kinetic curve of TCM and $C_3H_3Cl_3O$ showed the multi-step biphasic adsorption process. NR/HMS-SH reached to equilibrium plateau at 20 and 24 h, respectively. This probably related to the results from XRD that low degree of pore size distribution. While, the results showed that the four DBPs

concentration of PAC presented as same on the NR/HMS-SH. The kinetic curve of TCM and $C_3H_3Cl_3O$ showed the multi-step biphasic adsorption process, too. The PAC reaches equilibrium of DCAN, TCM and $C_3H_3Cl_3O$ at 2 h, 6 h and 6 h, respectively.

Three species of DBPs show adsorption capacity on NR/HMS-SH higher than adsorption on PAC but adsorption on PAC was reach within short contact time. This probably related to the low degree of porous structure as obtained by the XRD results.
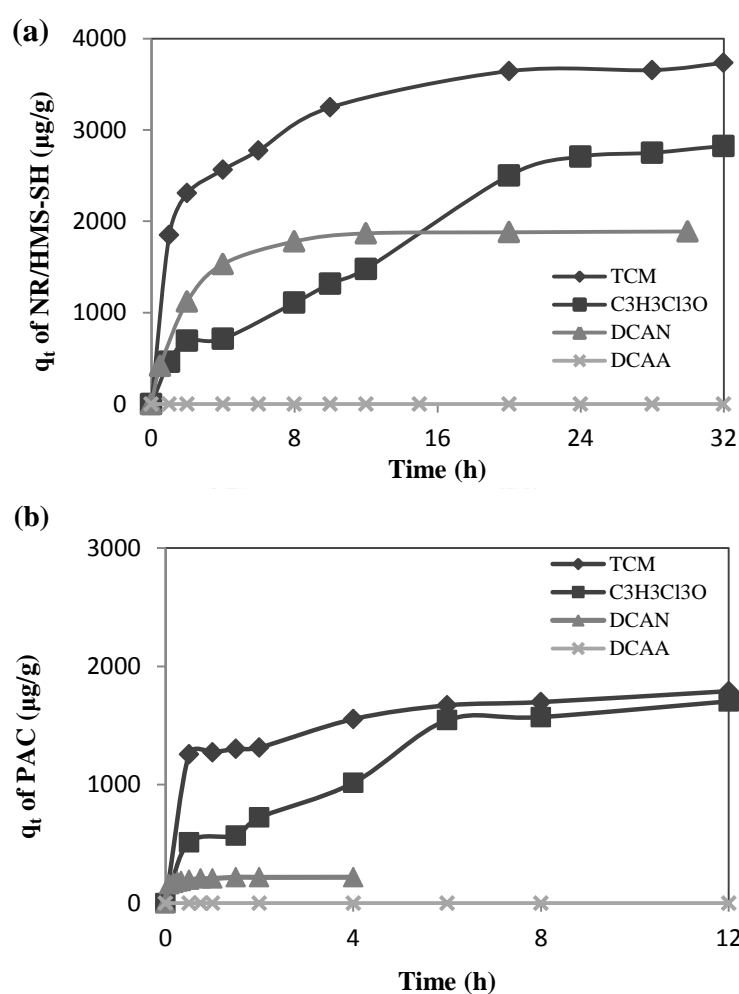
Figure 4.6 DBPs adsorption kinetics of (a) NR/HMS-SH at 1 mg/L and
(b) PAC at 0.5 mg/L, pH 7 and IS 10 nM

Adsorption kinetic models consist of pseudo-first-order and pseudo-second-order kinetic models were used to calculate the adsorption efficiency. The pseudo-first-order equation can be represented as followed in **Equation 4.1**

$$q_t = q_e(1 - exp^{(-k_1 t)}) \tag{4.1}$$

where q_e is the amount of adsorbed contaminant at equilibrium (µg/g), q_t is the amount of adsorbed contaminant at time (µg/g), and k_1 is rate constant of pseudo-first-order adsorption (min^{-1}). The values of k_1 and q_e can be calculated from the slope and intercept of the plot between 1/q and 1/t, respectively.

The pseudo-second-order model can be determined from following **Equation 4.2.**

$$\frac{t}{q_t} = \frac{1}{k_2 q_e^2} + \frac{t}{q_e} \tag{4.2}$$

Where k_2 is the rate constant of the pseudo-second-order adsorption (g/µg.min) that calculated from plots between t/q_t and t. The initial adsorption rate (h) can be determined in **Equation 4.3.**

$$h = k_2 q_e^2 \tag{4.3}$$

Table 4.3 Kinetic parameters of DCAN adsorption on NR/HMS-SH and PAC adsorbents

| Adsorbents | $q_{e,exp}$ (µg/g) | Pseudo-first-order | | | | Pseudo-second-order | | | | | |
		$q_{e,cal}$ (µg/g)	k_1 (min^{-1})	R^2	Δq (%)	$q_{e,cal}$ (µg/g)	k_2 (g/µg.min)	R^2	h (µg/g.min)	$t_{1/2}$ (min)	Δq (%)
NR/HMS-SH	1867	1793	0.0065	0.9895	49.94	2000	6.562 x 10^{-6}	0.9978	26.25	76.20	5.200
PAC	217.2	90.29	0.0425	0.8130	71.28	217.4	0.0017	0.9997	84.03	2.644	3.730

The calculated parameters for kinetic models of adsorbents (NR/HMS-SH and PAC) were shown in **Table 4.3 – 4.5.**

According to the kinetic parameters of DCAN, the correlation coefficients (R^2) of two models were showed in high values and were not significantly different as shown in **Table 4.3**. According to the normalized standard deviation (Δq) calculation of both models, the Δq value of pseudo-second models of both adsorbents were smaller than the pseudo-first-order model. Furthermore, the result showed that the initial rate adsorption (h) of DCAN adsorption on PAC was higher than adsorption on NR/HMS-SH that showed the higher adsorption affinity of DCAN.

The adsorption mechanism on adsorbent surface related to the driving force and surface area of the adsorbents. In this research, the driving force is adsorbate concentration and the amount of active sites on the surface of adsorbent is also the surface area. Consequently, the pseudo-second-order model is more suitable to describe the adsorptions kinetics of DCAN on both porous adsorbents. In the previous study, the results which related with this study was reported that the pseudo-second-order model was appropriate to explain the adsorption of low molecular weight compounds on small adsorbents particles.

Table 4.4 Kinetic parameters of TCM adsorption on NR/HMS-SH and PAC adsorbents

Adsorbents	$q_{e,exp}$ (µg/g)	Pseudo-first-order				Pseudo-second-order					
		$q_{e,cal}$ (µg/g)	k_1 (min^{-1})	R^2	Δq (%)	$q_{e,cal}$ (µg/g)	k_2 (g/µg.min)	R^2	h (µg/g.min)	$t_{1/2}$ (min)	Δq (%)
NR/HMS-SH	3644	2024	0.0026	0.9817	75.21	3333	3.321 x 10^{-6}	0.9986	36.90	90.33	16.40
PAC	1670.59	594.4	0.0063	0.9012	90.64	2000	1.344 x 10^{-5}	0.9976	53.76	37.20	14.71

The kinetic parameters of TCM were shown in **Table 4.4**. The correlation coefficients (R^2) of two models were showed in high values. The R^2 values in pseudo-second models of both adsorbents were higher than the pseudo-first-order model. Therefore, the adsorptions of TCM on both adsorbents were suitable for pseudo-second-order model. Furthermore, the result showed that the initial rate adsorption (h) of TCM adsorption on PAC was higher than adsorption on NR/HMS-SH that showed the higher adsorption affinity of TCM.

Table 4.5 Kinetic parameters of $C_3H_3Cl_3O$ adsorption on NR/HMS-SH and PAC adsorbents

Adsorbents	$q_{e,exp}$ (µg/g)	Pseudo-first-order				Pseudo-second-order					
		$q_{e,cal}$ (µg/g)	k_1 (min^{-1})	R^2	Δq (%)	$q_{e,cal}$ (µg/g)	k_2 (g/µg.min)	R^2	h (µg/g.min)	$t_{1/2}$ (min)	Δq (%)
NR/HMS-SH	2709.45	2827.59	0.0018	0.8452	52.24	2344.89	1.747×10^{-7}	0.8709	4.369	1144	25.18
PAC	1545.17	1036.91	0.004	0.9297	67.62	1456.31	2.706×10^{-6}	0.9382	10.82	184.8	20.11

Table 4.5 showed the kinetic parameters of $C_3H_3Cl_3O$ on both adsorbents NR/HMS-SH and PAC found that the correlation coefficients (R^2) of pseudo-second-order models of both adsorbents were nearly. From the values of the normalized standard deviation (Δq) calculation of both models, the Δq value of pseudo-second models of both adsorbents were smaller than the pseudo-first-order model. Thereby, the adsorptions of $C_3H_3Cl_3O$ on both adsorbents were appropriated with pseudo-second-order model to explain the adsorption process same as the adsorption of DCAN and TCM. Moreover, the initial rate adsorption (h) values of $C_3H_3Cl_3O$ on PAC were higher than adsorption on NR/HMS-SH that showed the higher adsorption affinity of $C_3H_3Cl_3O$.

In the case of adsorption kinetic curve for DCAA on the NR/HMS-SH and PAC, they cannot conclude the adsorption capacity of DCAA on both adsorbents. It might because of the surface properties of adsorbents such as the high hydrophobicity which might show the poor adsorption for DCAA because of its positive charge.

4.2.2   Intraparticle Diffusion Machanism

The adsorption process on porous material adsorbents includes three steps. The first step is film diffusion process, the second step is particle diffusion process and the last step is adsorption of the adsorbate onto active sites on the surface of adsorbent. The last step is step that can be negligible because this step is very fast when compared with two steps above. Therefore, the film diffusion or intraparticle diffusion step are also the rate limiting step of adsorption process.

Intraparticle diffusion model used to analyze from kinetic data to predict rate-controlling step in adsorption process. It can be determined as **Equation 4.4.**

$$q_t = k_i t^{\frac{1}{2}} + C \qquad\qquad (4.4)$$

Where q_t is the amount of adsorbate adsorbed (mg/g) at time $t^{1/2}$ ($min^{1/2}$), k_i is the intraparticle diffusion rate constant ($mg/g.min^{1/2}$) and C is the interception. It can be determined from the plot of q_t vs $t^{1/2}$.
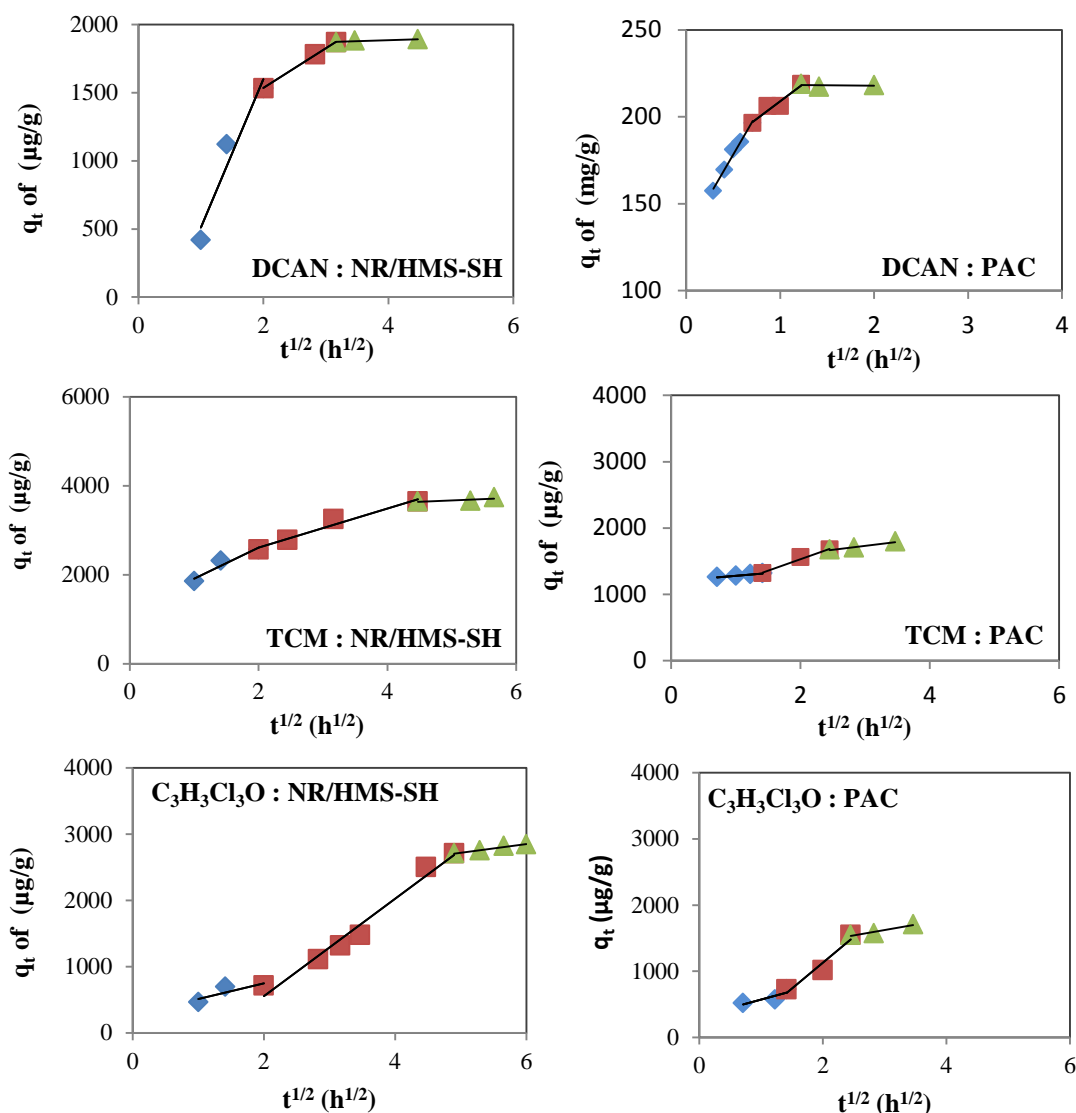
Figure 4.7 Intraparticle diffusion plots of DBPs (DCAN, TCM and $C_3H_3Cl_3O$) onto NR/HMS-SH and PAC

    The fitting curves for the adsorption DBPs (DCAN, TCM and $C_3H_3Cl_3O$) onto NR/HMS-SH and PAC as showed in **Figure 4.7**. They presented multi-linearity that indicating the multiple steps of adsorption process. The first step represented the external mass transfer in the boundary layer that can be determined the rate constant from the slope of first regime while the second step presented the diffusion of DBPs

into the internal of adsorbent that can be indicated the rate constant from the second regime; and the last step showed the adsorption of DBPs on internal site of adsorbent.

.
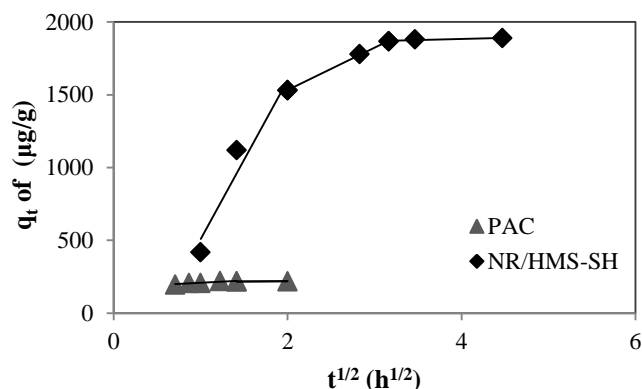
Figure 4.8 Intraparticle diffusion plots of DCAN onto NR/HMS-SH and PAC

First of all, the plotting of DCAN adsorption on NR/HMS-SH and PAC did not across the origin as shown in **Figure 4.8.**

They showed multi-linearity that refers to the multiple step of adsorption. The 1st step presented the external mass transfer in the boundary layer; the 2nd step showed the diffusion of DCAN into the internal of adsorbent. It can be indicated the rate constant from the 1st and 2nd regime of the curves, respectively. Moreover, the last step presented the DCAN adsorption on internal site of adsorbent. It very fast occurred. The rate limiting step of the adsorption was been the 1st or 2nd step. Both steps of adsorption can be the controlling step together. The intraparticle diffusion model parameters of DCAN adsorption on adsorbents were shown in **Table 4.6**

Table 4.6 Intraparticle diffusion model parameters of DCAN adsorption on
NR/HMS-SH and PAC adsorbents

Adsorbents	1st stage			2nd stage		
	k_i $(mg/g.h^{1/2})$	C	R^2	k_i $(mg/g. h^{1/2})$	C	R^2
NR/HMS-SH	1087	-576.9	0.9398	291.2	950.9	0.9993
PAC	93.30	131.7	0.9878	40.90	168.1	0.9399

Secondly, the intraparticle diffusion model of TCM adsorption on NR/HMS-SH and PAC was shown in **Figure 4.9**
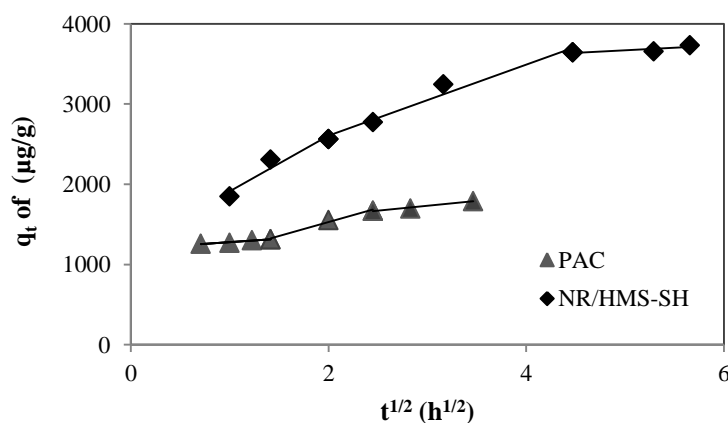
Figure 4.9 Intraparticle diffusion plots of TCM onto NR/HMS-SH and PAC

According to the fitting curves as showed in **Figure 4.9**, they presented multi-linearity in the multiple step of adsorption. The first step can be determined the rate constant from the slope of first regime; the second step can be indicated the rate constant from the second regime of the curves; and the last step was the adsorption of TCM on internal site of adsorbent which can be negligible due to its very rapidly occurring. So, the rate limiting step of the adsorption can be the first or second step. The plotting of TCM adsorptions on both adsorbents did not across the origin means

that the rate limiting step is not only intraparticle diffusion. Thus, the controlling step can be both intraparticle and film diffusion steps together. The intraparticle diffusion model parameters of TCM adsorption on adsorbents were shown in **Table 4.7**.

Table 4.7 Intraparticle diffusion model parameters of TCM adsorption on NR/HMS-SH and PAC adsorbents

Adsorbents	1st stage			2nd stage		
	k_i $(\mu g/g.h^{1/2})$	C	R^2	k_i $(\mu g/g. h^{1/2})$	C	R^2
NR/HMS-SH	695.5	1216	0.9334	441.8	1723	0.9691
PAC	83.33	1196	0.9707	347.3	834.3	0.9850

Finally, the intraparticle diffusion model of $C_3H_3Cl_3O$ adsorption on NR/HMS-SH and PAC was shown in **Figure 4.10.**

The all regime represented the step of adsorption like an adsorption on DCAN and TCM. In generally, the first step and second step happened together and the second step should be slower than first step. It mean that slope of the second step should be less than the first step. In this study showed unusually results. The rate limiting step was the film diffusion and/or intraparticle diffusion step. Moreover, the final step was able to neglect due to its rapidly occurring. Moreover, the curves showed that the adsorption of $C_3H_3Cl_3O$ on both adsorbents did not pass through the origin, so the limiting step can be 1st and 2nd step of the adsorption. The intraparticle diffusion model parameters of TCM adsorption on NR/HMS-SH and PAC were shown in **Table 4.8**.
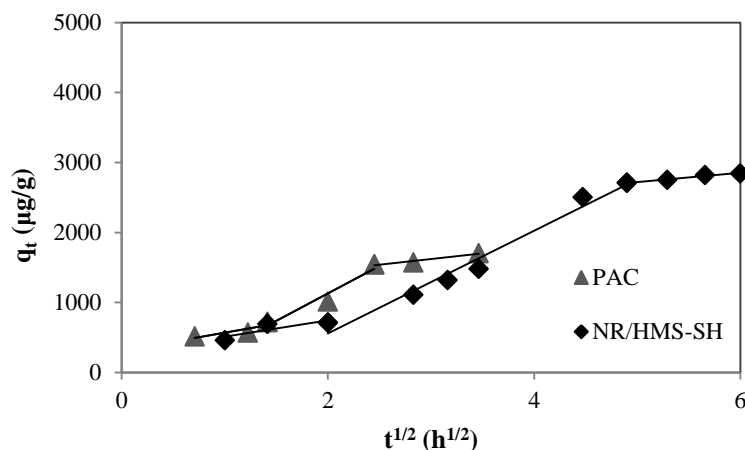
Figure 4.10 Intraparticle diffusion plots of $C_3H_3Cl_3O$ onto NR/HMS-SH and PAC

Table 4.8 Intraparticle diffusion model parameters of $C_3H_3Cl_3O$ adsorption on NR/HMS-SH and PAC adsorbents

Adsorbents	1st stage			2nd stage		
	k_i $(mg/g.h^{1/2})$	C	R^2	k_i $(mg/g.h^{1/2})$	C	R^2
NR/HMS-SH	236.9	274.3	0.7277	734.3	-910.3	0.9756
PAC	256.6	315.5	0.7489	779.7	-429.6	0.9428

4.2.3   Adsorption Isotherm

4.2.3.1 Adsorption isotherm of HANs in single solute solution

The adsorption capacities of HANs on NR/HMS-SH compared with PAC are shown in **Figure 4.11.** The data for HANs adsorption on both adsorbents are plotted with different Y-axis scale because of much high adsorption capacity. The adsorption capacities MCAN on NR/HMS-SH were slightly less than on PAC whereas DCAN and TCAN adsorption capacity on NR/HMS-SH was lower than PAC. TCAN show the high adsorption capacity more than DCAN and MCAN, respectively.

According to the molecules of adsorbate, HANs adsobate are neutral molecules, however the positive charge and negative dipole in atom of each HANs can be interact with the surface functional groups of adsorbent. The surface of NR/HMS-SH exhibited a negative charge at pH 7 (pH_{PZC} = 5.46). Furthermore, this result suggests that hydrophobic surface of NR/HMS-SH and PAC show high adsorption capacity by reducing the competitive adsorption between water and HANs onto the adsorbents. Therefore, the much high adsorption capacity of NR/HMS-SH and PAC can be describe to the combination of hydrophobic surface and the thiol-group giving the ion-dipole interaction.
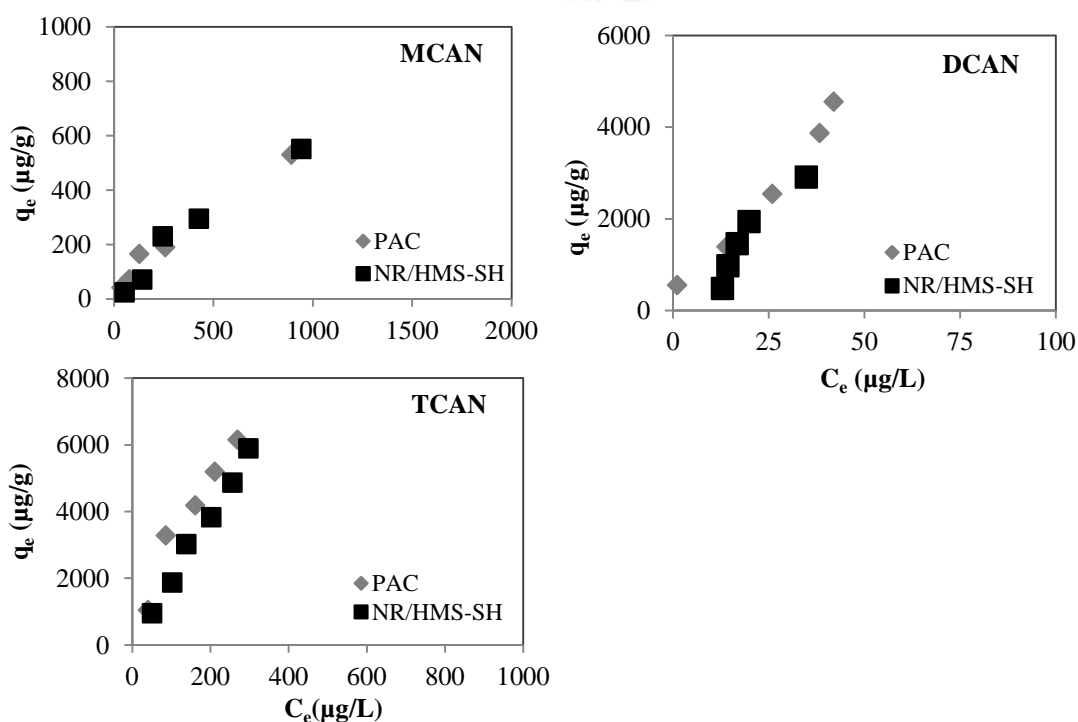
Figure 4.11 Comparison of adsorption capacities of MCAN, DCAN and TCAN on NR/HMS-SH and PAC at pH 7 and IS 10 mM

Moreover, HANs in single solution was observed the adsorption capacity that showed in the **Figure 4.12.** As seen in the **Figure 4.12 (a),** the single adsorption isotherm for three different HANs adsorbates by NR/HMS-SH showed order as following; TCAN > DCAN > MCAN. DCAN and TCAN had a high adsorption capacities compared with MCAN on NR/HMS-SH because they had the high molecular weight that exhibited higher adsorption capacities. The results suggest that the adsorption capacities of three HANs on synthesized adsorbent are related to the molecule structure of HANs. The results showed as same as the previous study of (Prarat et. al., 2011) about adsorption of HANs onto M-HMS that conclude that TCAN give higher adsorption capacities than DCAN and MCAN, respectively. Moreover, the single adsorption isotherm for three different HANs adsorbates by PAC as shown in **Figure 4.12 (b)** showed order as following; TCAN > DCAN > MCAN that same adsorption on NR/HMS-SH but it shown as a different from previous study in the order of TCAN and DCAN. It might be related to molecular weight or solubility.
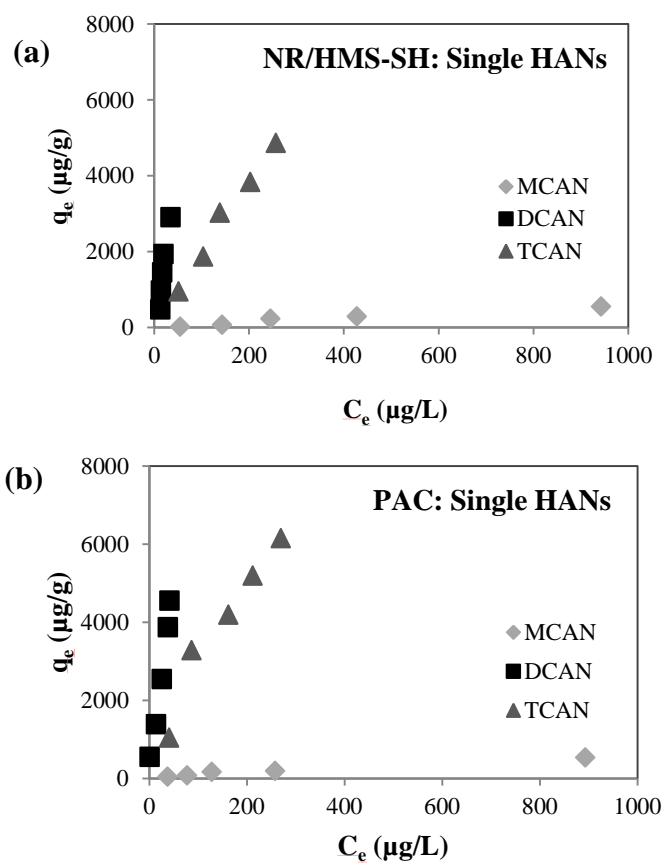
Figure 4. 12 Adsorption isotherm of three HANs as (a) single solute on NR/HMS-SH and (b) single solute on PAC at pH 7 and IS 10 mM

4.2.3.2 Adsorption isotherm of TCM in single solute solution
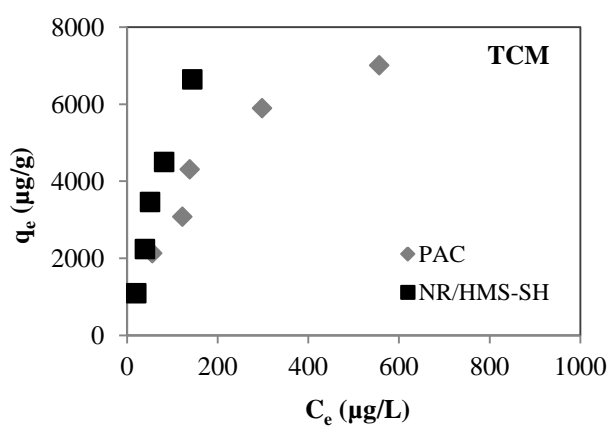
Figure 4.13 Comparison of adsorption capacities of TCM on NR/HMS-SH and PAC at pH 7 and IS 10 mM

According to **Figure 4.13** that shown the adsorption capacities of TCM on NR/HMS-SH compared with PAC, the adsorption capacities of TCM on NR/HMS-SH was higher than on PAC.

4.2.3.3 Adsorption isotherm of $C_3H_3Cl_3O$ in single solute solution

The adsorption capacities of $C_3H_3Cl_3O$ on NR/HMS-SH compared with PAC are shown in **Figure 4.14.** The adsorption capacities $C_3H_3Cl_3O$ on NR/HMS-SH was higher than that for PAC.
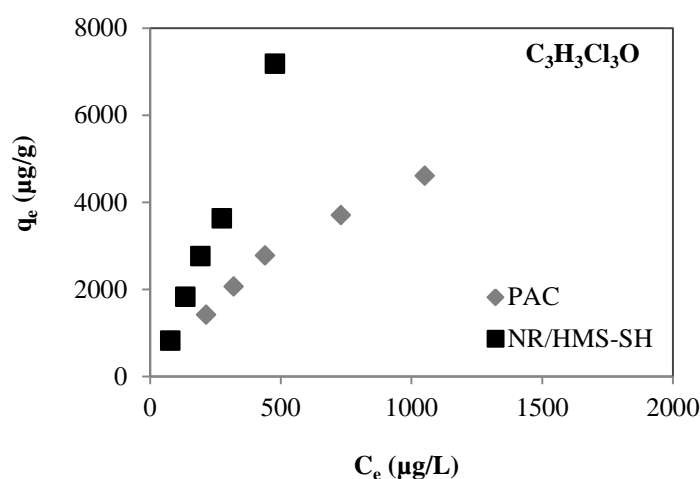
Figure 4.14 Comparison of adsorption capacities of $C_3H_3Cl_3O$ on NR/HMS-SH and PAC at pH 7 and IS 10 mM

4.2.4   Isotherm Models

The isotherm models, which are Linear, Langmuir and Freundlich isotherm were used to calculate the adsorption isotherm. The linear isotherm shows relationship between concentration of adsorbate and the amount of adsorbate that adsorbed at the equilibrium. This isotherm can be shown in the following **Equation 4.5.**

$$q_e = K_p C_e \tag{4.5}$$

where q_e is the amount of adsorbate that adsorbed at the equilibrium (µg/g), K_p is linear constant (L/µg), and C_e is concentration of adsorbate at equilibrium (µg/L). The Langmuir isotherm of linear form can be written in the **Equation 4.6.**

$$\frac{1}{q_e} = \frac{1}{K_L q_m C_e} + \frac{1}{q_m} \tag{4.6}$$

where q_e is the amount of adsorbate that adsorbed at the equilibrium (µg/L), q_m is the maximum adsorption capacity (µg/g), K_L is the Langmuir constant (L/µg). The Freundlich isotherm of linear form can be written as **Equation 4.7.**

$$\ln(q_e) = \ln(K_F) + \frac{1}{n}\ln(C_e) \tag{4.7}$$

where K_F and n are constants, and C_e is the equilibrium concentration (µg/L). Moreover, the value of K_F and n depend on temperature, the nature of adsorbent and the adsorbate property.

4.2.4.1 Isotherm models of HANs adsorption

Figure 4.15 shows the adsorption isotherm of HANs on NR/HMS-SH and PAC. Adsorption of MCAN and DCAN on NR/HMS-SH presented the linear model by considering the highly correlation coefficient value (R^2) in **Table 4.9** whereas TCAN that the Freundlich model showed the best fitting. For PAC, DCAN and TCAN presented the linear model that supported by the high R^2 values while MCAN fitted with the Langmuir model.

Figure 4.15 Comparison of the predicted and experimental data for the equilibrium adsorption of HANs on NR/HMS-SH and PAC at pH 7

Table 4.9 Isotherm parameters of Linear, Langmuir and Freundlich models for adsorption of HANs in single solute on NR/HMS-SH and PAC (pH 7 and 10 mM)

Isotherms	HANs		
	MCAN	DCAN	TCAN
NR/HMS-SH			
Linear			
K_p	0.5805	100.0	19.52
R^2	0.9586	0.8960	0.9901
Δq (%)	70.83	43.37	1620.03
Langmuir			
q_m ($\mu g\ g^{-1}$)	-	-	-
K_L ($L\ \mu g^{-1}$)	-	-	-
R^2	-	-	-
Δq (%)	-	-	-
Freundlich			
n	0.8828	0.6331	0.9709
K_F ($\mu g\ g^{-1}$)	3.417	13.03	16.60
R^2	0.9563	0.7904	0.9909
Δq (%)	1258	35.22	6.193
PAC			
Linear			
K_p	0.5449	97.07	20.57
R^2	0.9785	0.9825	0.9424
Δq (%)	37.57	22.11	30.39
Langmuir			
q_m ($\mu g\ g^{-1}$)	1000	3333	-
K_L ($L\ \mu g^{-1}$)	0.0010	0.1764	-
R^2	0.9818	0.9394	-
Δq (%)	16.01	41.68	-
Freundlich			
n	1.256	1.802	1.121
K_F ($\mu g\ g^{-1}$)	2.484	458.1	45.21
R^2	0.9653	0.9297	0.9345
Δq (%)	16.35	52.97	16.75

4.2.4.2 Isotherm models of TCM adsorption

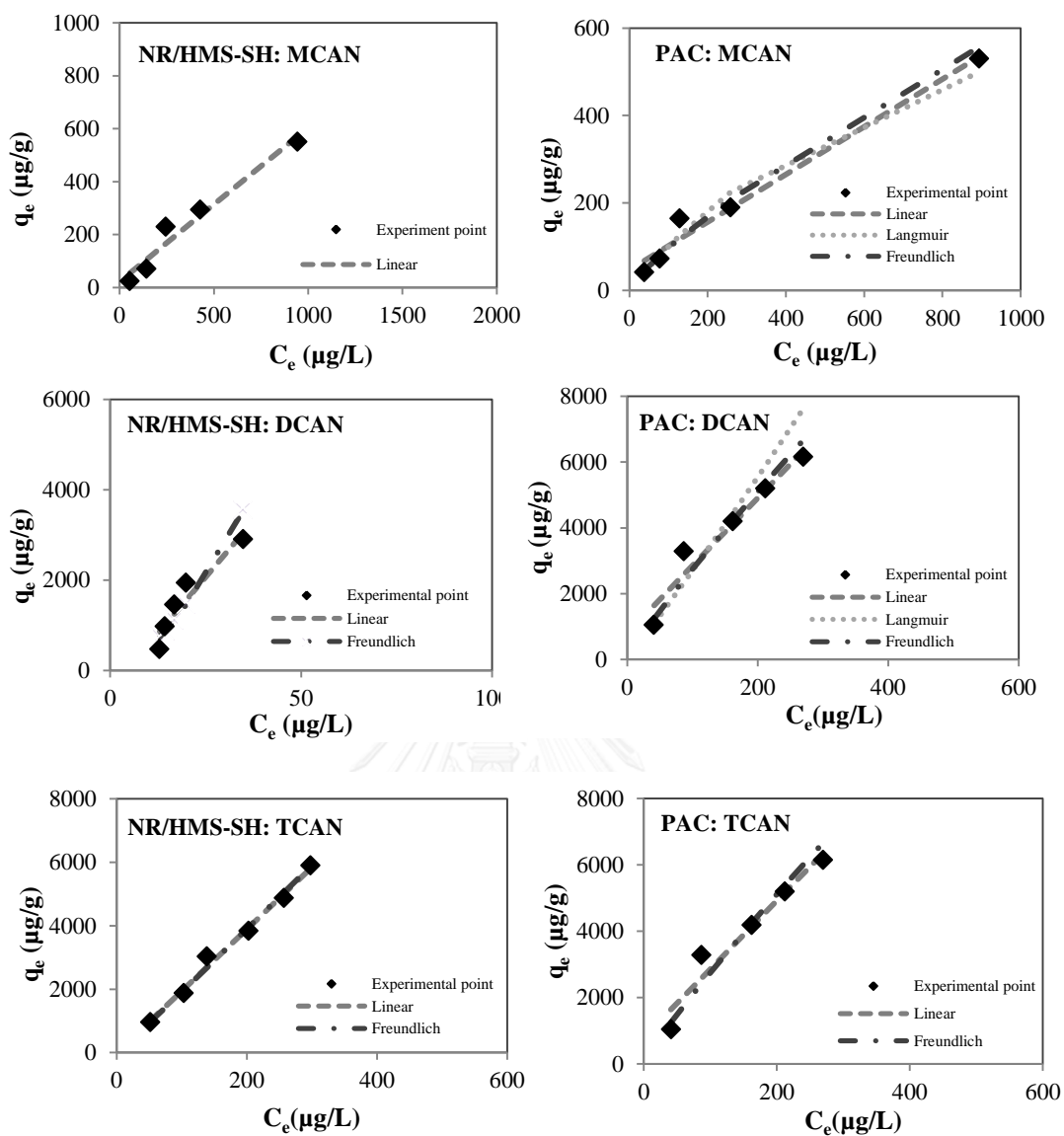**Figure 4.16** Comparison of the predicted and experimental data for the equilibrium
adsorption of TCM on NR/HMS-SH and PAC at pH 7

According to **Figure 4.16** and **Table 4.10**, the adsorption of TCM on PAC
presented the Langmuir model by considering the highly correlation coefficient value
(R^2). The result revealed that the adsorption of TCM on adsorbents occurred on
homogeneous surface of adsorbents and can be limited on monolayer surface with no
transmigration of adsorbate in the plane surface. For adsorption of TCM on NR/HMS-
SH fitted with Freundlich isotherm.

Table 4.10 Isotherm parameters of Linear, Langmuir and Freundlich models for adsorption of TCM in single solute on NR/HMS-SH and PAC (pH 7 and 10 mM)

Isotherms	TCM
NR/HMS-SH	
Linear	
K_p	43.17
R^2	0.9605
Δq (%)	23.48
Langmuir	
q_m ($\mu g\ g^{-1}$)	-
K_L ($L\ \mu g^{-1}$)	-
R^2	-
Δq (%)	-
Freundlich	
n	1.079
K_F ($\mu g\ g^{-1}$)	73.74
R^2	0.9658
Δq (%)	12.42
PAC	
Linear	
K_p	9.262
R^2	0.8738
Δq (%)	20.70
Langmuir	
q_m ($\mu g\ g^{-1}$)	10000
K_L ($L\ \mu g^{-1}$)	0.0048
R^2	0.9571
Δq (%)	11.08
Freundlich	
n	1.880
K_F ($\mu g\ g^{-1}$)	264.2
R^2	0.9422
Δq (%)	11.29

4.2.4.3 Isotherm models of C₃H₃Cl₃O adsorption

The adsorption isotherm parameters of $C_3H_3Cl_3O$ on NR/HMS-SH and PAC were shown in **Figure 4.17** and **Table 4.11**. These shown that the adsorption of $C_3H_3Cl_3O$ on NR/HMS-SH fitted with linear model while adsorption on PAC presented the data that best fitted with Langmuir model by following R^2 values.
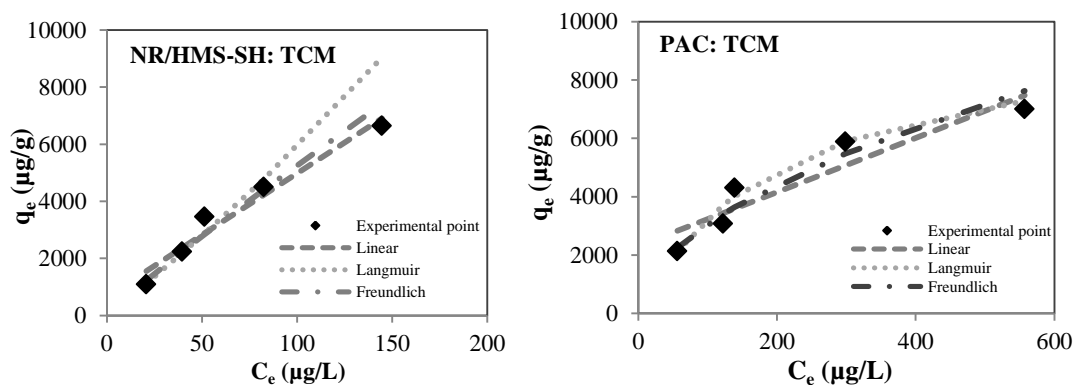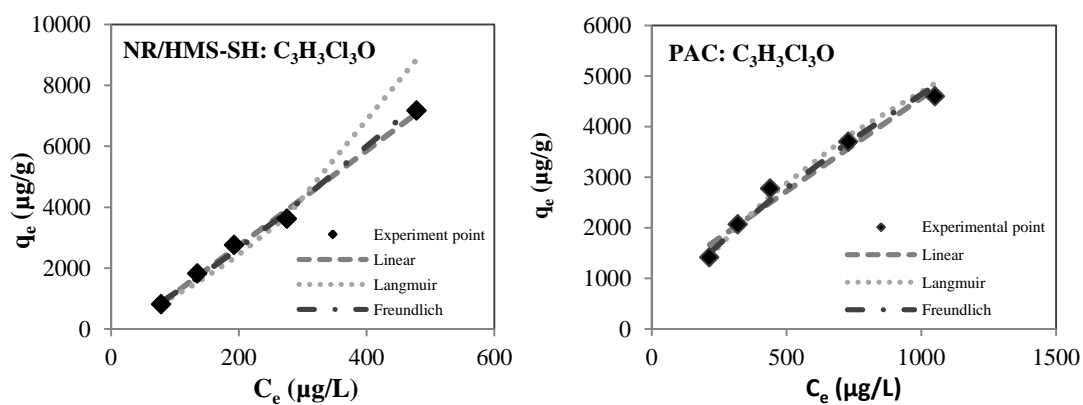

Figure 4.17 Comparison of the predicted and experimental data for the equilibrium adsorption of $C_3H_3Cl_3O$ on NR/HMS-SH and PAC at pH **7**

Table 4.11 Isotherm parameters of Linear, Langmuir and Freundlich models for adsorption of $C_3H_3Cl_3O$ in single solute on NR/HMS-SH and PAC (pH 7 and 10 mM)

Isotherms	$C_3H_3Cl_3O$
NR/HMS-SH	
Linear	
K_p	15.59
R^2	0.9948
Δq (%)	5.772
Langmuir	
q_m ($\mu g\ g^{-1}$)	-
K_L ($L\ \mu g^{-1}$)	-
R^2	-
Δq (%)	-
Freundlich	
n	0.855
K_F ($\mu g\ g^{-1}$)	5.384
R^2	0.99
Δq (%)	8.031
PAC	
Linear	
K_p	3.693
R^2	0.9718
Δq (%)	10.63
Langmuir	
q_m ($\mu g\ g^{-1}$)	12500
K_L ($L\ \mu g^{-1}$)	6.038 x 10^{-4}
R^2	0.9945
Δq (%)	4.365
Freundlich	
n	1.363
K_F ($\mu g\ g^{-1}$)	29.21
R^2	0.9838
Δq (%)	5.906

4.2.5   Adsorption Selectivity

Figure 4.18 showed the adsorption isotherm of fours DBPs in single solute solution and mixed solute solution on NR/HMS-SH and PAC. Clearly, NR/HMS-SH could efficiently adsorbed TCM and $C_3H_3Cl_3O$ in the presence of co-existing DBPs in single solution. As seen in the **Figure 4.18 (a)**, the single adsorption isotherms for the four types of DBPs adsorbates by NR/HMS-SH were ranked in the adsorption preference order of TCM > DCAN > $C_3H_3Cl_3O$ > DCAA, while DBPs adsorption with NR/HMS-SH in mixed solute solution were ranked as following $C_3H_3Cl_3O$ > TCM > DCAA > DCAN. The results in mixed solution represented the lower adsorption capacity than results in single solute solution except DCAN that shown the results did not same in the previous studies which were ranked DCAN > TCM > DCAA.

In case of DCAA, it cannot was adsorbed with NR/HMS-SH in single solution but the adsorption capacity of DCAA shown higher value than adsorption in mixed solution cause by complexity of functional group.

It can concluded the adsorption isotherm of DBPs on NR/HMS-SH and PAC in the mixed solutes of all DBPs adsorbate results indicated that three species affected to the adsorption efficiency of each DBPs by decreasing adsorption capacity except DCAA adsorption and it can be concluded that DCAN might has lowest competitive to interact with the active surface of NR/HMS-SH. It might related to the hydrophobic interaction (in case of TCM and $C_3H_3Cl_3O$) took place faster than ion-dipole interaction of DCAN case.

However, on PAC the order of adsorption capacities nearly like in the single adsorbate, being DCAN > TCM > $C_3H_3Cl_3O$ > DCAA. DCAN had highest adsorption capacity followed by TCM, $C_3H_3Cl_3O$ and DCAA, respectively as shown in **Figure 4.18 (b).** It can represent that the adsorption capacities of TCM and DCAA with PAC showed higher than adsorption with synthesized material. It might be caused of the surface complexity of functional group of PAC which may induce varies interaction such as van der Waals force towards TCM, $C_3H_3Cl_3O$, DCAA and DCAN adsorption.
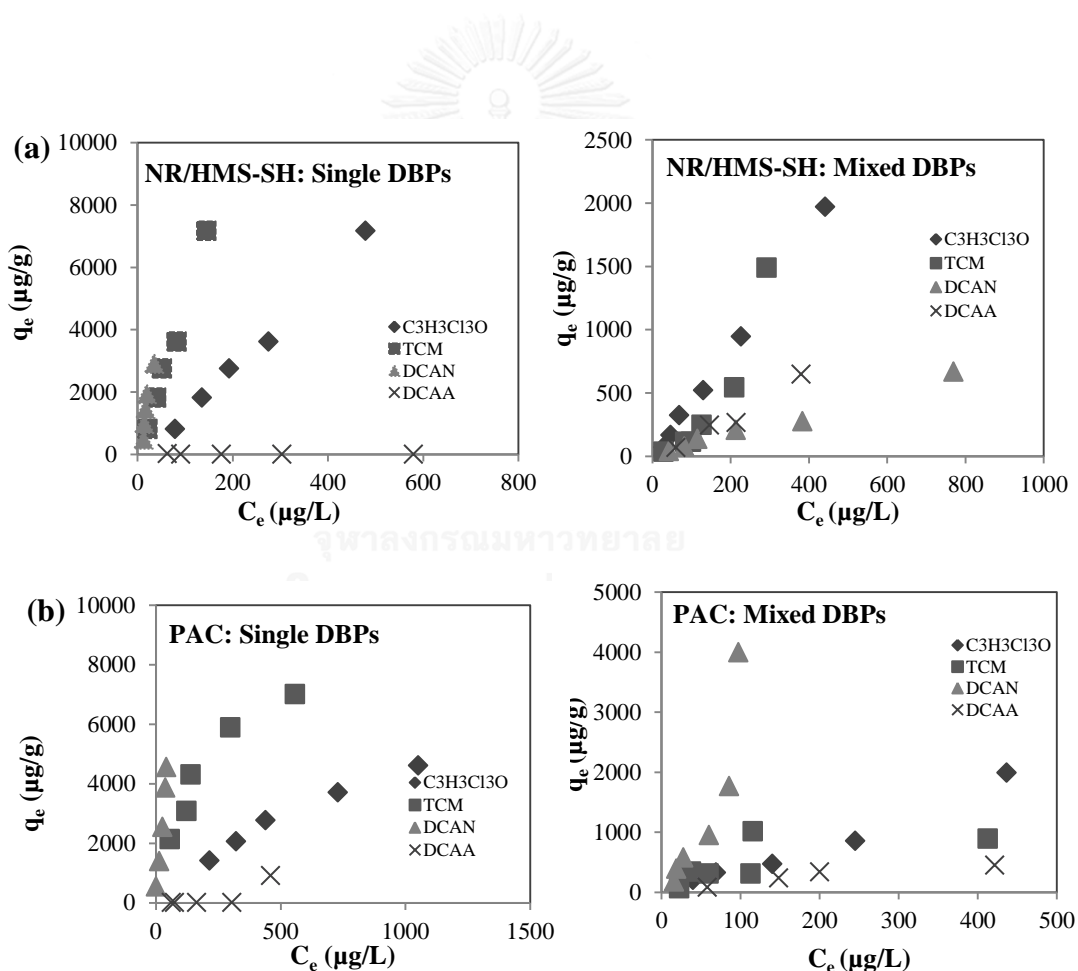

Figure 4.18 Adsorption isotherms of DBPs as a single solute solution and mixed solute solution on (a) NR/HMS-SH and (b) PAC at pH 7 with IS 10 mM

4.2.6   Effects of NOM on DCAN adsorption capacity

The effect of NOM on DCAN adsorption was studied. The tap water from laboratory of the International Postgraduate program in Hazardous Substance and Environmental Management, Chulalongkorn University was used as background water sample in this study. Before using, water sample was fractionated into two fraction of NOM are hydrophobic NOM (HPO) and hydrophilic NOM (HPI) by fractionation of ion exchange resin. The TOC results can be presented that hydrophilic DOC was 2.731 mg C/L, hydrophobic DOC was 2.456 mg C/L (10 times concentrated) while in total DOC in tap water was 2.759 mg C/L.
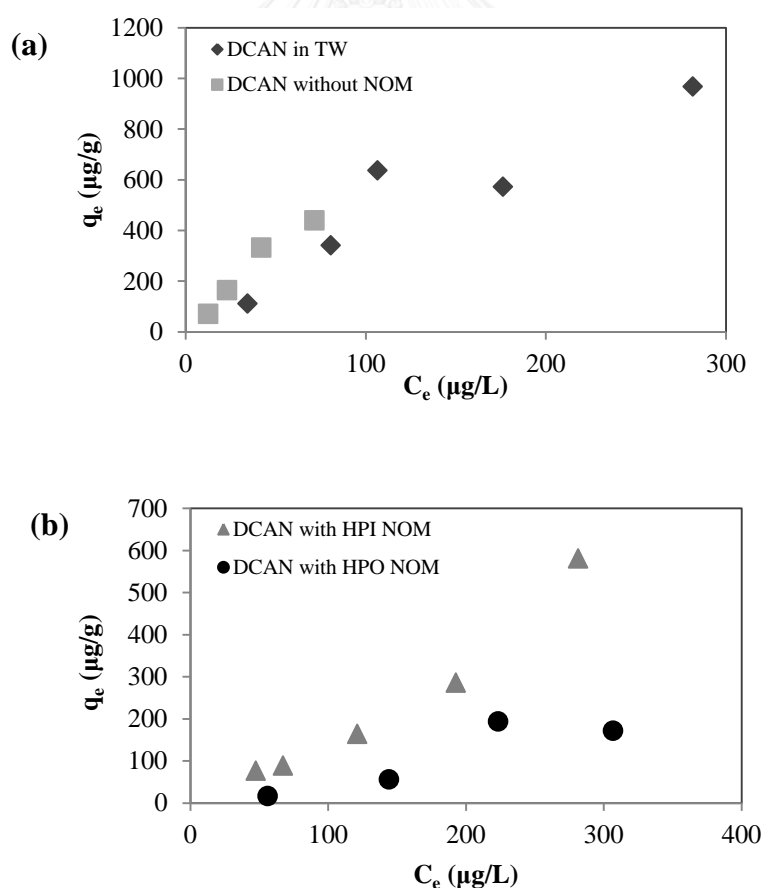

Figure 4.19 Effect of NOM on DCAN adsorption capacity of NR/HMS-SH

The adsorption of DCAN with tap water comparing with the adsorption of DCAN showed in **Figure 4.19 (a)**. The result showed that the presence of DCAN in tap water can decrease DCAN adsorption capacity. It might be caused the adsorption competition and pore blocking onto the adsorbent surface.

Furthermore, the result in **Figure 4.19 (b)** showed that DCAN adsorption capacity with HPO NOM was lower than HPI NOM. It might be caused of the adsorption competition between DCAN and HPO NOM on NR/HMS-SH that had hydrophobic surface.
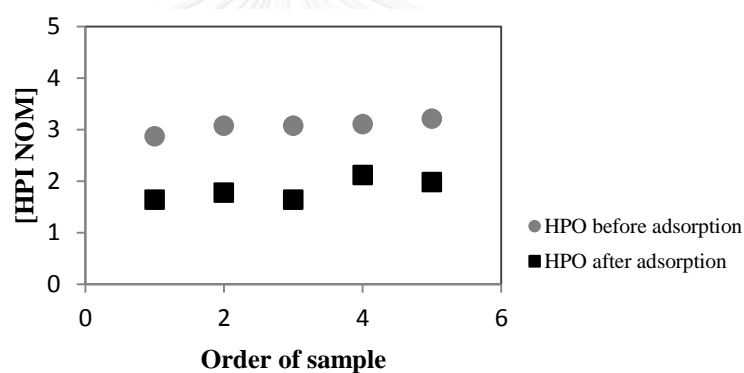
Figure 4.20 Effect of hydrophobic NOM on DCAN adsorption capacity
of NR/HMS-SH
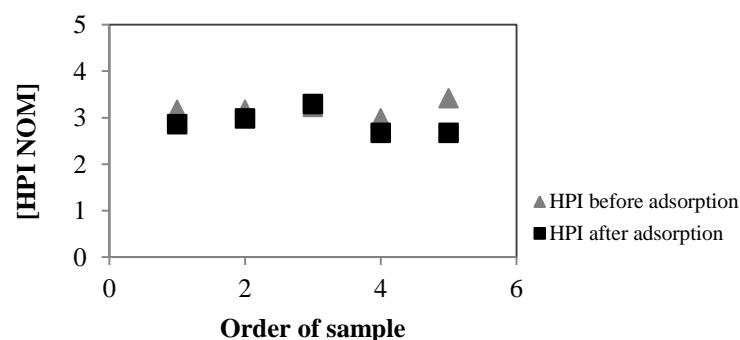
Figure 4.21 Effect of hydrophilic NOM on DCAN adsorption capacity
of NR/HMS-SH

The adsorption competition between DCAN can be confirmed by **Figure 4.20** that presented HPO concentration which was decreased from initial concentration after adsorption. HPO NOM might be block pore of adsorbent that caused to decreasing of the active sites on surface of adsorbent resulting from the lower adsorption capacity of DCAN. Moreover, HPO NOM might be interacting with adsorbent via hydrophobic interaction. On the other hand, HPI NOM and tap water did not prefer the decreasing capacity on the adsorbent as presented in **Figure 4.21** and. **Figure 4.22.**

Figure 4.22 Effect of tap water on DCAN adsorption capacity of NR/HMS-SH

CHAPTER V

CONCLUSION AND RECOMMENDATIONS

5.1   CONCLUSION

According to the adsorption kinetic study of DBPs including HANs, TCM, $C_3H_3Cl_3O$ and HAAs on thiol-functionalized mesoporous composites based on natural rubber and hexagonal meso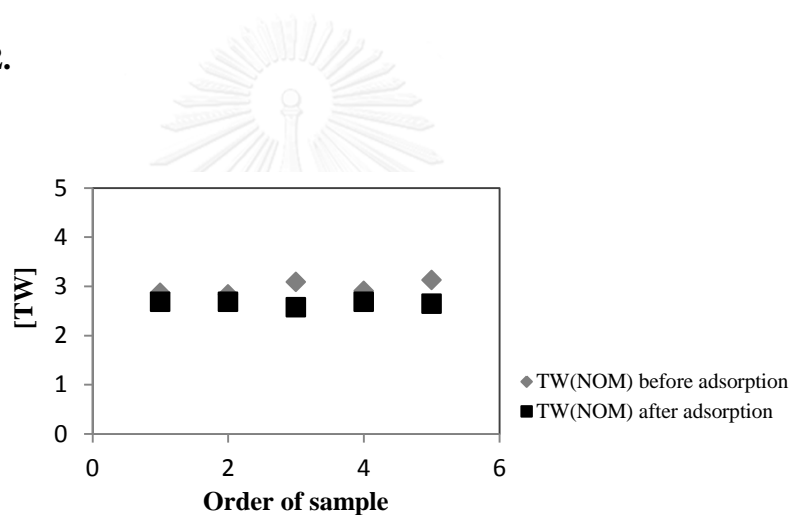porous silicates (NR/HMS-SH) comparing with powder activated carbon (PAC) presence that the data of all kinetic adsorption were suitable for describe by the pseudo-second-order model excepted the adsorption kinetic of DCAA that cannot determine adsorption capacity on both adsorbents. The adsorption capacities of DBPs on synthesized adsorbent are nearly on the PAC.

Moreover, the intraparticle model of the adsorptions, these can indicate to the multiple step of adsorption, and the rate limiting step of the adsorption was shown in the film diffusion or intraparticle diffusion step. The part of adsorption isotherm, DBPs adsorption isotherm presented the data fitting with many isotherm models depending on the characteristic of each DBP.

Furthermore, the single adsorption isotherms for the four types of DBPs adsorbates by NR/HMS-SH were ranked of TCM > DCAN > $C_3H_3Cl_3O$ > DCAA, while in mixed solute solution were ranked as following $C_3H_3Cl_3O$ > TCM > DCAA > DCAN. The results in mixed solution showed the lower adsorption capacity than results in single solute solution as same as on PAC the order of adsorption capacities nearly like in the single adsorbate, being DCAN > TCM > $C_3H_3Cl_3O$ > DCAA. The species of DBPs in the mixed solute solution affected to the adsorption capacity

comparing with the single solution. The adsorption isotherm of DBPs on NR/HMS-SH and PAC in the mixed solutes of all DBPs adsorbate indicated that three species affected to the adsorption efficiency of each DBPs by decreasing adsorption capacity except DCAA adsorption which cause by complexity of functional group and in case of DCAN might has lowest competitive to interact with the active surface of NR/HMS-SH. It might relate to the hydrophobic interaction.

The adsorption of DCAN with HPO showed the concentration of DCAN decreased from initial concentration after adsorption and it had lower efficiency when HPO appeared in the system because of the competitive of active site on adsorbent surface and pore blocking which caused to decreasing of the active sites on surface of adsorbent resulting from the lower adsorption capacity of DCAN and HPO NOM might be interacting with adsorbent via hydrophobic interaction.

5.2   RECOMMENDATION

1. This synthesized adsorbent should be investigated and improved the stability of adsorbents during use in real unit operation.

2. The adsorption experiments should be applied for on other adsorbent such as HMS-SH and NR/HMS.

3. Mass transfer parameters should be calculated for design of the fixed bed column.

4. The study of Effect NOM in tap water should be uses various source of tap water.

5. Regeneration method and reuse efficiency should be investigated.

REFERENCES

Babi, K. G., K. M. Koumenides, A. D. Nikolaou, C. A. Makri, F. K. Tzoumerkas and T. D. Lekkas (2007). Pilot study of the removal of THMs, HAAs and DOC from drinking water by GAC adsorption. *Desalination 210*(1-3): 215-224.

Cancho, B., F. Ventura and M. T. Galceran (1999). Behavior of Halogenated Disinfection By-Products in the Water Treatment Plant of Barcelona, Spain. *Bullein of Environmental Contamination and Toxicology 63*: 610-617.

Dickey, F. H. (1949). Preparation of specific adsorbents. Paper presented at the Proceedings of the national academy of sciences.

EPA_Method_551.1 (1990). Determination of Chlorination Disinfection Byproducts, Chlorinated Solvents and Halogenated Pesticides/herbicides in Drinking Water by Liquid-Liquid Extraction and Gas Chromatography with Electron-capture Detection, National Exposure Research Laboratory, Office of Research and Development, U.S. Environmental Protection Agency, Cincinnati, OHIO.

EPA_Method_552.2 (1990). Determination of Haloacetic Acids and Dalapon in Drinking Water by Liquid-Liquid Extraction and Gas Chromatography with Electron-capture Detection, National Exposure Research Laboratory, Office of Research and Development, U.S. Environmental Protection Agency, Cincinnati, OHIO.

Glueckauf, E.(1955). Theory of chromatography. *Trans Faraday Soc.*, 51, 1540.

Hepplewhite, C., Newcombe, G., and Knappe, D. R. U. (2004). NOM and MIB, Who Wins in the Competition for Activated Carbon Adsorption Sites?. *Water Science and Technology, 49(9):* 257-265.

Kim, J. and B. Kang (2008). DBPs removal in GAC filter-adsorber *Water Rearch 42*: 145-152.

Lebeaua, T., Lelièvrea, C., Wolbertb, D., Laplancheb, A., Pradosa, M., and Côté, P. (1999). Effect of natural organic matter loading on the atrazine adsorption capacity of an aging powdered activated carbon slurry. *Water Research 33(7):* 1695–1705.

Marhaba, T. F., and Washington, M. B. (1998). Drinking water disinfection and by-

products: history and current practice. *Adv. Environ. Res., 2(1):* 103-115.

Matsui, Y., Fukuda Y., Inoue, T. and Matsushita, T. (2003). Effect of natural organic matter on powdered activated carbon adsorption of trace contaminants: characteristics and mechanism of competitive adsorption. *Water Research 37(18):* 4413-24.

Nlkolaou, A., S. Golfinopoulos, L. Rizzo, G. Lofrano, T. Lekkas and V. Belgiomo (2005). Optimization of analytical methods for the determination of DBPs: Application to drinking waters from Greece and Italy *Desalination 176*: 25-36

Nuntang, S., S. Poompradub, S. Butnark, T. Yokoi, T. Tatsumi and C. Ngamcharussrivichai (2014). Novel mesoporous composites based on natural rubber and hexagonal mesoporous silica: Synthesis and characterization *Materials Chemistry and Physics 143*: 1199-1208.

Okwu, U.N. and Okieimen, F.E. (2001). Preparation and properties of thioglycollic acid modified epoxidised natural rubber and its blends with natural rubber. *European Polymer Journal 37(11)*: 2253-2258.

Owen, D. M., Amy, G. L., and Chowdhury, Z. K. (1993). NOM characterization and treatability. *J.AWWA, 75(10):* 46-63.

Prarat, P., C. Ngamcharussrivichai, S. Khaodhiar and P. Punyapalakul (2011). Adsorption characteristics of haloacetonitriles on functionalized silica-based porous materials in aqueous solution. *J Hazard Mater 192*(3): 1210-1218.

Pruttisirikula, T., Prasassarakichb, P., Rempelc, G. L., Hinchiranan, N. (2010). Thioacetate- and mercapto-functionalized hydrogenated natural rubber. *Reactive and Functional Polymers 70(9)*: 674–683.

Punyapalakul, P. and S. Takizawa (2006). Selective adsorption of nonionic surfactant on hexagonal mesoporous silicates (HMSs) in the presence of ionic dyes. *water research 40*(17): 3177-3184.

Rakruam, P. and Wattanachira, S. (2014). Reduction of DOM fractions and their trihalomethane formation potential in surface river water by in-line coagulation with ceramic membrane filtration *Journal of Environmental Sciences 26*: 529-536

Ratasuk, C., C. Kositanont and C. Ratanatamskul (2008). Removal of haloacetic acids by ozone and biologically active carbon. *ScienceAsia 34*(3): 293-298.

Tanev, P. T., and Chibwe, M. (1994). Titanium-containing mesoporous molecular sieves for catalytic oxidation of aromatic compounds Nature, *368:* 321-323.

Tung, H.-H., R. F. Unz and Y. F. Xie (2006). HAA removal by GAC adsorption. *Journal of American Water Works Association 98*: 107-112.

Uyak, V., I. Koyuncu, I. Oktem, M. Cakmakci and I. Toroz (2008). Removal of trihalomethanes from drinking water by nanofiltration membranes. *J Hazard Mater 152*(2): 789-794.

Uyak, V., S. Yavuz, I. Toroz, S. Ozaydin and E. A. Genceli (2007). Disinfection by-products precursors removal by enhanced coagulation and PAC adsorption. *Desalination 216*: 334–344.

Vaiopoulou, E., T. M. Misiti and S. G. Pavlostathis (2015). Removal and toxicity reduction of naphthenic acids by ozonation and combined ozonation-aerobic biodegradation. *Bioresour Technol 179*: 339-347.

Wang, G. S. Effects of natural organic matter on adsorption capacity for atrazine by activated carbon (2005). *Journal of the Chinese Institute of Environmental Engineering 15(2):* 81-89.

APPENDIX

APPENDIX A
Standard Calibration Curves
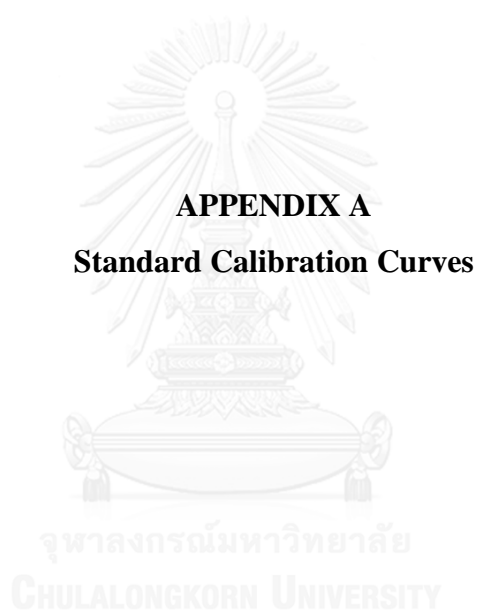
1. Preparation of disinfection by-products (DBPs) stock solution 500 mg/L

Table A-1   The volume of stock DBPs at concentration 500 mg/L

DBPs	Volume of DBPs (µL)	Total volume (mL)
MCAN	4.2	10
DCAN	3.7	10
TCAN	3.5	10
TCM	3.4	10
$C_3H_3Cl_3O$	3.7	10
DCAA	3.2	10

All DBPs at volume that showed in the table were dissolved in deionized water (DI) by using micropipette to adjust the volume.

Then, the stock solution 500 mg/L of DBPs were diluted to 1 mg/L with DI water in 100 mL of volumetric flask by calculation as shown in **Equation A-1**.

$$C_1V_1 = C_2V_2 \hspace{2cm} (A\text{-}1)$$

Example Preparation of 1 mg/L DCAN from stock solution 500 mg/L in 100 mL of volumetric flask

$$C_1V_1 = C_2V_2$$

$$500 \text{ mg/L} . V_1 = 1 \text{ mg/L} . 100 \text{ mL}$$

$$V_1 = 0.2 \text{ mL}$$

So, pipetted stock solution of DCAN 0.2 mL into 100 mL of volumetric flask and adjusted volume of solution by phosphate buffer (PB) 10 mM until 100 mL

2.   Preparation of DBPs standard concentration

Then, preparation of DBPs standard concentration (in µg/L) by diluting from the stock solution 1 mg/L of DBPs in 25 mL of volumetric flask by calculation from Equation A-1.

Table A-2   Volume of stock DBPs 1 mg/L to prepare the standard concentration

Concentration of DBPs (µg/L)	Volume of stock 1 ppm (mL)
1	0.0250
5	0.1250
25	0.6250
50	1.250
100	2.500
150	3.750
200	5.000
250	6.250

Moreover, the preparation of DBPs standard concentration from stock solution 500 mg/L of DBPs in 25 mL of volumetric flask can calculate from Equation A-1.

Table A-3   Volume of stock DBPs 500 mg/L to prepare the standard concentration

Concentration of DBPs (µg/L)	Volume of stock 500 ppm (µL)
500	25.00
750	37.50
1000	50.00
1250	62.50
1500	75.00
2000	100.0

3. Standard curve

The concentrations of standard solution of DBPs were analyzed by GC/µECD with VF-X column. Standard curve was plotted between peak area and concentration of standard solution of DBPs.
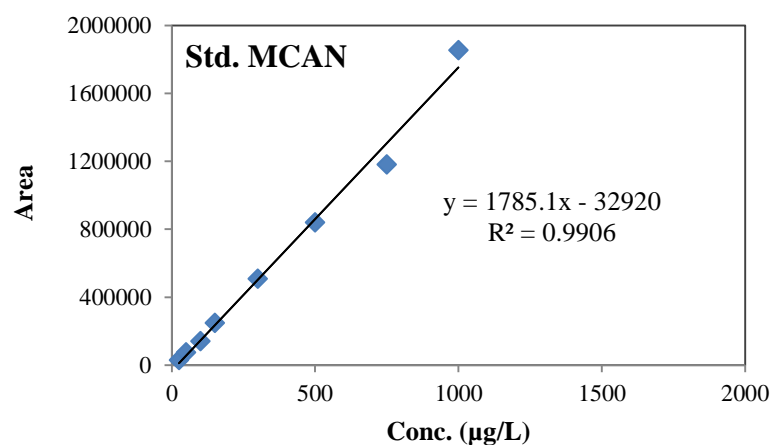

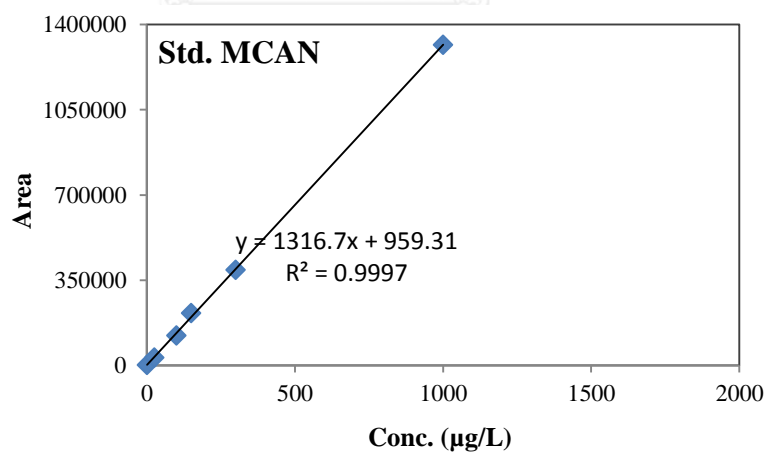**Figure A-1**   Standard curve of MCAN on NR/HMS-SH

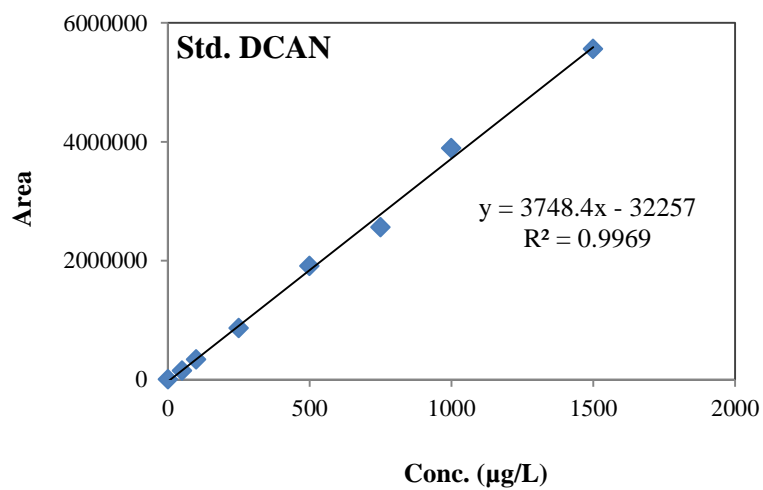**Figure A-2**   Standard curve of MCAN on PAC

Figure A-3   Standard curve of DCAN on NR/HMS-SH

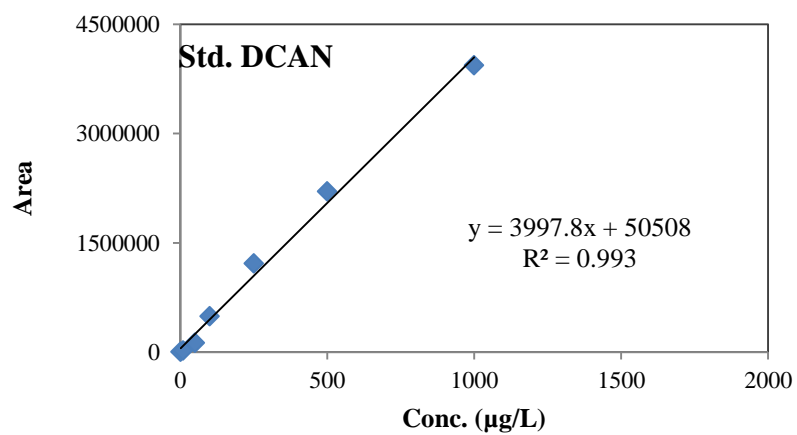**Figure A-4**   Standard curve of DCAN on PAC

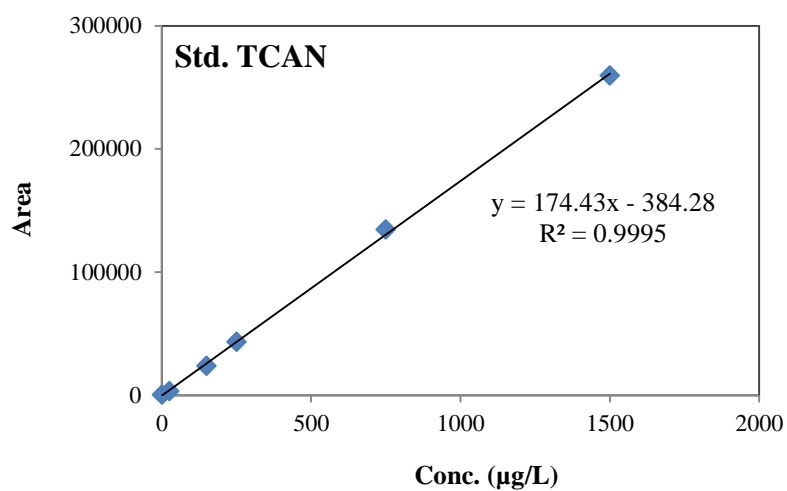**Figure A-5**   Standard curve of TCAN on NR/HMS-SH
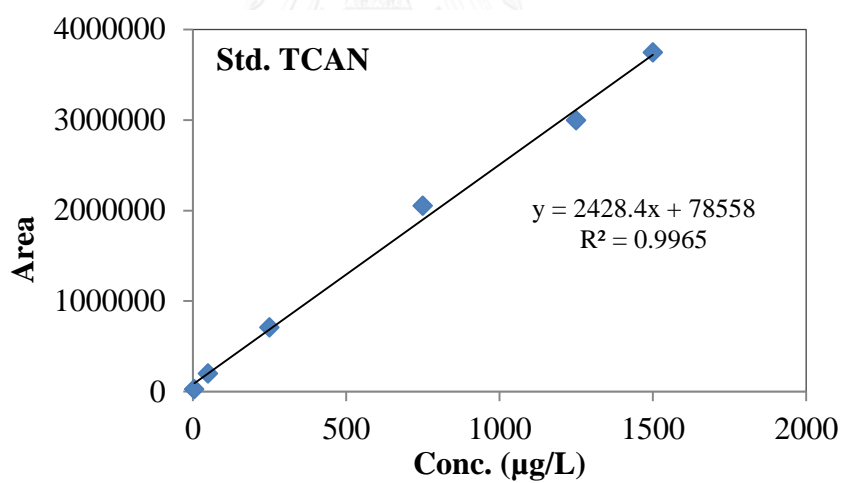

Figure A-6   Standard curve of TCAN on PAC
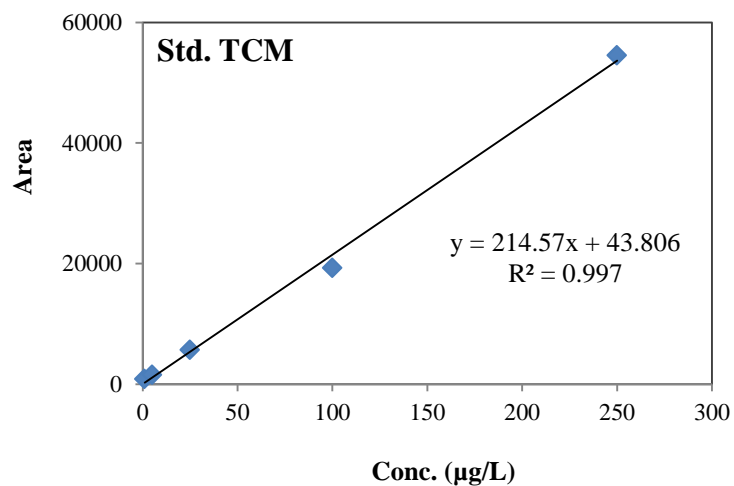
Figure A-7   Standard curve of TCM on NR/HMS-SH and PAC
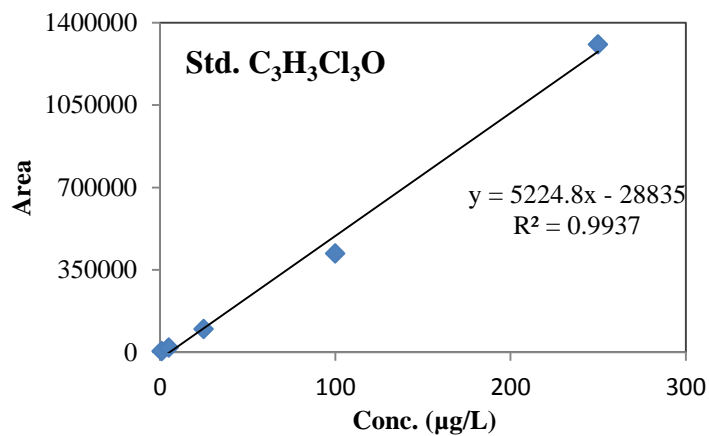
Figure A-8   Standard curve of $C_3H_3Cl_3O$ on NR/HMS-SH and PAC
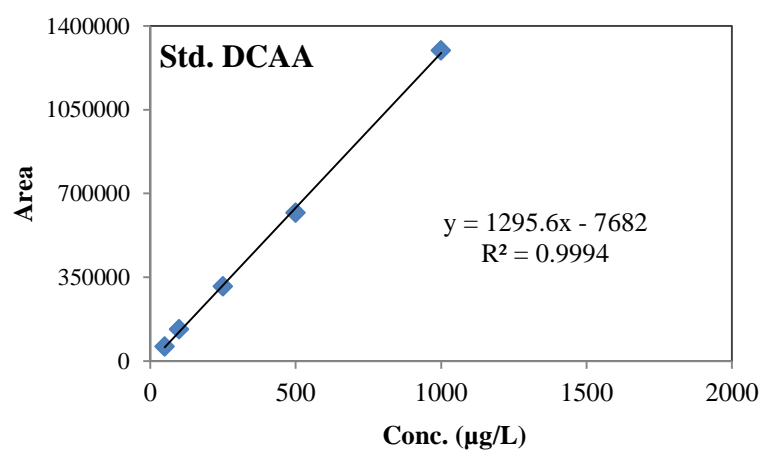
Figure A-9   Standard curve of DCAA on NR/HMS-SH and PAC

APPENDIX B

Data of Physicochemical Characterization of Adsorbents

1. Surface charge density investigation by Acid-Base titration

Table B-1   Data from calculation of surface charge density of NR/HMS-SH

Sample	pH	Surface charge (C/m^2)
1	3.78	0.0037
2	4.22	0.0044
3	4.51	0.0021
4	4.87	0.0013
5	5.51	0.0008
6	5.57	0.0003
7	5.46	-0.0001
8	5.6	-0.0005
9	5.61	-0.0008
10	5.71	-0.0013
11	5.74	-0.0029
12	6.11	-0.0055
13	6.77	-0.0109
14	6.80	-0.0219

Table B-2   Data from calculation of surface charge density of PAC

Sample	pH	Surface charge (C/m^2)
1	6.36	0.0274
2	6.44	0.0149
3	6.61	0.0074
4	6.71	0.0036
5	6.83	0.0015
6	6.91	0.0007
7	6.92	0.0004
8	6.94	-0.0004
9	6.96	-0.0007
10	7.00	-0.0014
11	7.03	-0.0037
12	7.09	-0.0074
13	7.15	-0.0149
14	7.19	-0.0298

จุฬาลงกรณ์มหาวิทยาลัย
CHULALONGKORN UNIVERSITY

APPENDIX C

Data of Adsorption Kinetics
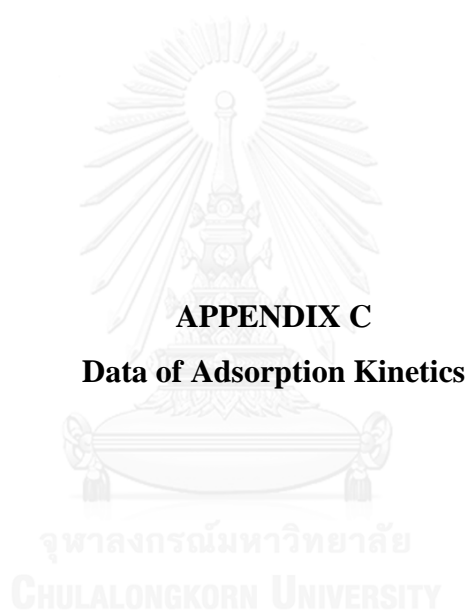
1. Adsorption kinetic study

Table C-1   Data from Adsorption kinetic of DCAN, TCM, C$_3$H$_3$Cl$_3$O, and DCAA on NR/HMS-SH (pH 7 and IS 10 mM)

DCAN		TCM		C$_3$H$_3$Cl$_3$O		DCAA	
t (min)	q$_t$ (µg/g)	t (min)	q$_t$ (µg/g)	t (min)	q$_t$ (µg/g)	t (min)	q$_t$ (µg/g)
0	0.000	0	0.000	0	0.000	0	0
30	417.2	30	207.5	60	462.2	60	0
120	1119	60	191.4	120	693.0	120	0
240	1532	90	373.7	240	713.5	240	0
480	1779	120	398.7	480	1108	360	0
720	1867	240	420.8	600	1317	480	0
1200	1880	360	435.7	720	1479	600	0
1800	1889	480	451.9	1200	2502	720	0
		720	496.9	1440	2709	900	0
				1680	2750	1200	0
				1920	2821	1440	0
				2160	2845	1680	0

Table C-2   Data from Adsorption kinetic of DCAN, TCM, C$_3$H$_3$Cl$_3$O, and DCAA on PAC (pH 7 and IS 10 mM)

DCAN		TCM		C$_3$H$_3$Cl$_3$O		DCAA	
t (min)	q$_t$ (µg/g)	t (min)	q$_t$ (µg/g)	t (min)	q$_t$ (µg/g)	t (min)	q$_t$ (µg/g)
0	0.000	0	0.000	0	0.000	0	0.00
5	157.4	30	1258	30	513.2	30	0
10	169.6	60	1273	90	569.1	45	0
15	181.1	90	1302	120	722.9	60	0
20	185.5	120	1314	240	1014	120	0
30	196.4	240	1554	360	1545	240	0
45	206.1	360	1670	480	1572	360	0
60	206.2	480	1699	720	1705	480	0
90	218.9	720	1791			720	0
120	217.2						
240	218.2						

Figure C-1   Plotted pseudo-first-order of DCAN on NR/HMS-SH

(pH 7 and IS 10 mM)

Figure C-2   Plotted pseudo-second-order of DCAN on NR/HMS-SH

(pH 7 and IS 10 mM)

Figure C-3   Plotted pseudo-first-order of DCAN on PAC

(pH 7 and IS 10 mM)

Figure C-4   Plotted pseudo-second-order of DCAN on PAC
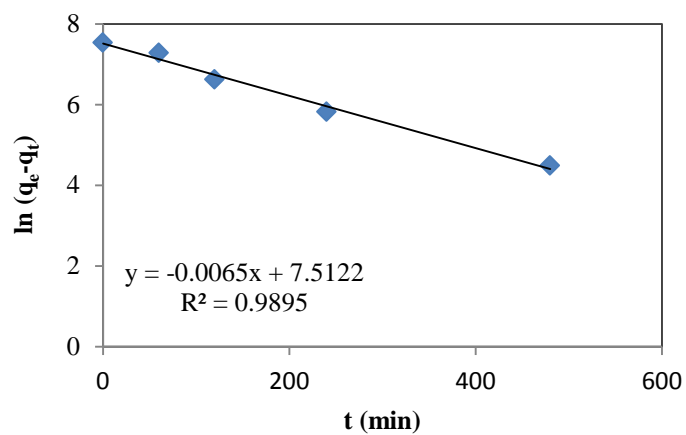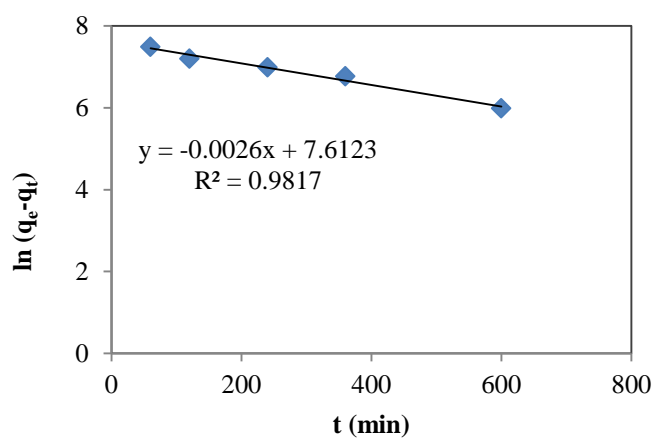
(pH 7 and IS 10 mM)

Figure C-5   Plotted pseudo-first-order of TCM on NR/HMS-SH
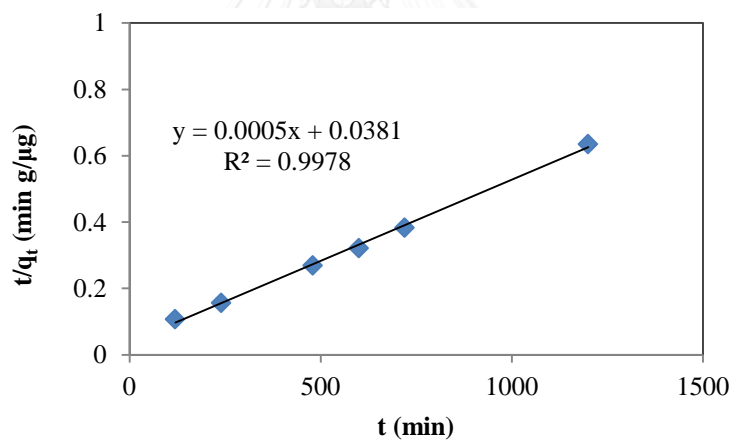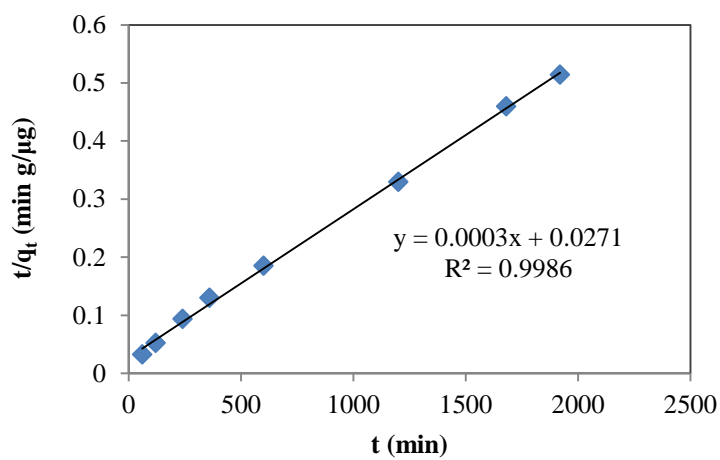
(pH 7 and IS 10 mM)

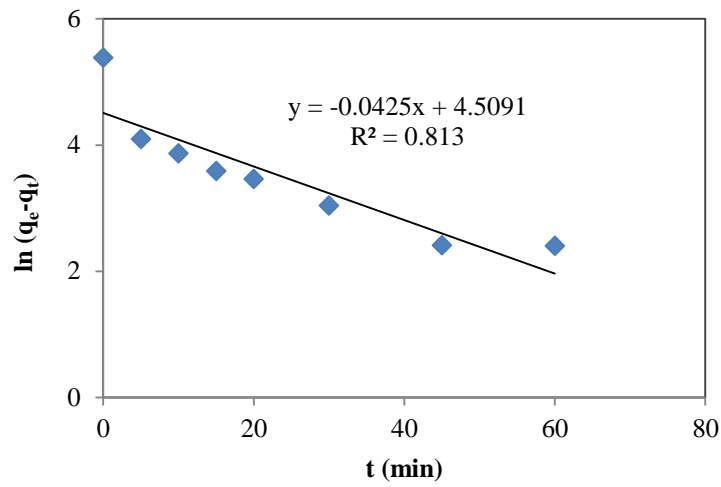**Figure C-6**   Plotted pseudo-second-order of TCM on NR/HMS-SH
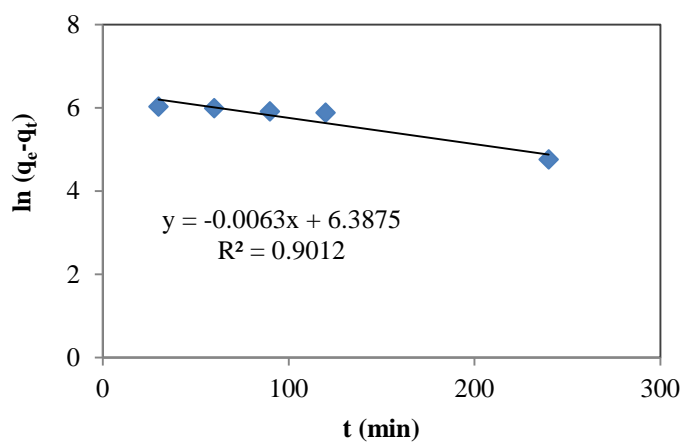
(pH 7 and IS 10 mM)

Figure C-7   Plotted pseudo-first-order of TCM on PAC
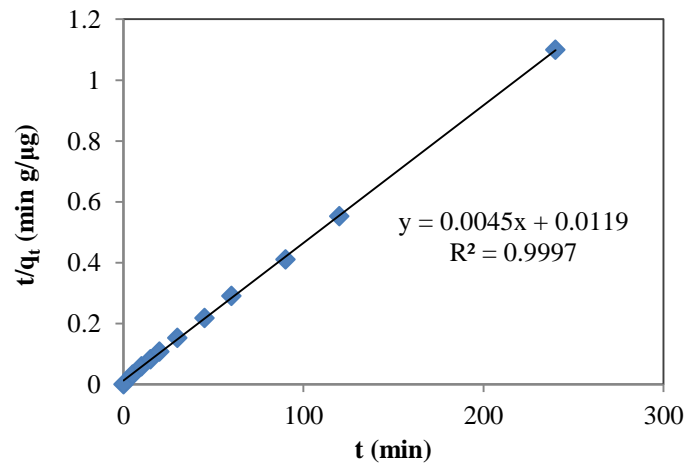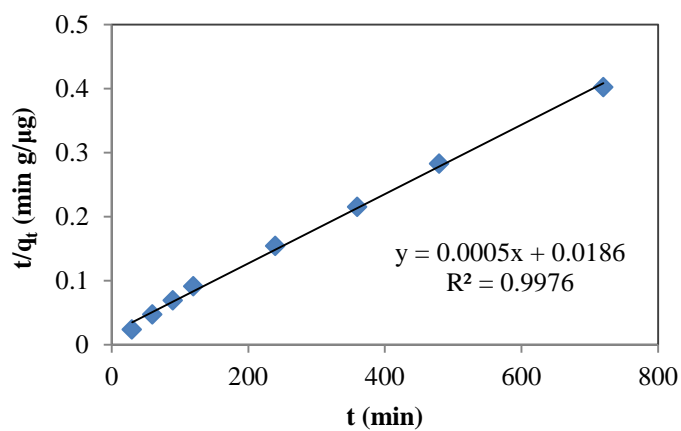
(pH 7 and IS 10 mM)

Figure C-8   Plotted pseudo-second-order of TCM on PAC

(pH 7 and IS 10 mM)

Figure C-9 Plotted pseudo-first-order of $C_3H_3Cl_3O$ on NR/HMS-SH

(pH 7 and IS 10 mM)

Figure C-10 Plotted pseudo-second-order of $C_3H_3Cl_3O$ on NR/HMS-SH

(pH 7 and IS 10 mM)

Figure C-11   Plotted pseudo-first-order of $C_3H_3Cl_3O$ on PAC

(pH 7 and IS 10 mM)

Figure C-12   Plotted pseudo-second-order of $C_3H_3Cl_3O$ on PAC
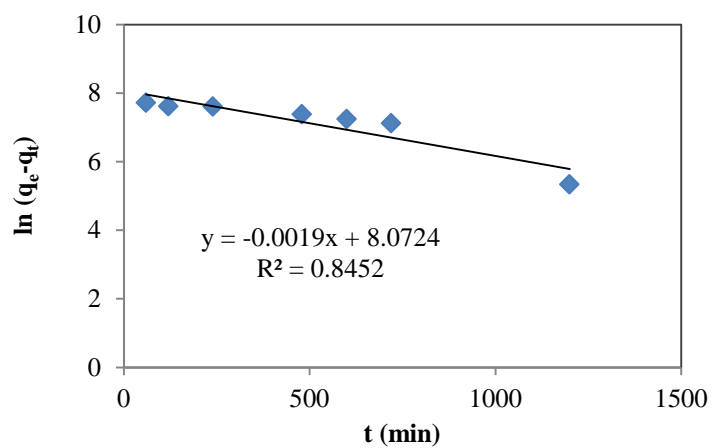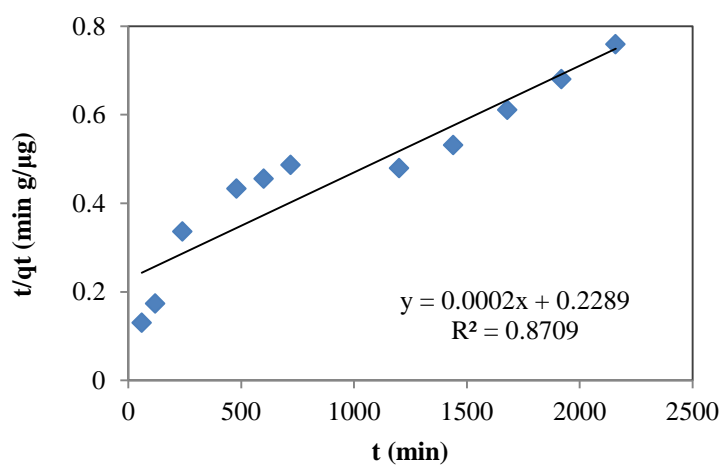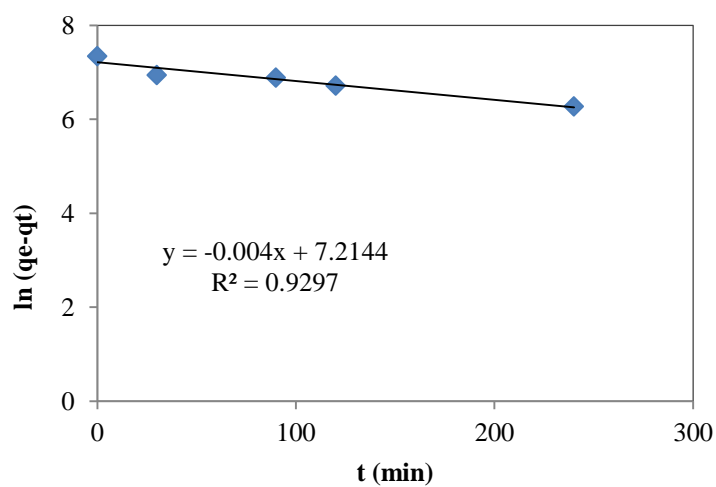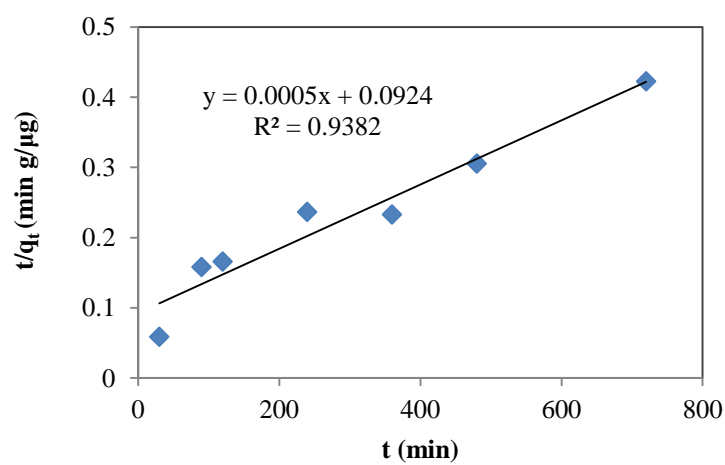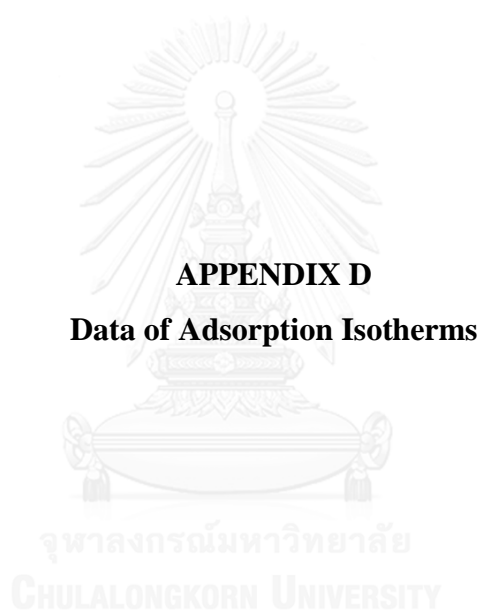
(pH 7 and IS 10 mM)

APPENDIX D

Data of Adsorption Isotherms

1. Adsorption isotherm study

Table D-1 Data from adsorption isotherms of three-HANs, TCM, $C_3H_3Cl_3O$, and DCAA on NR/HMS-SH in single solution (pH 7 and IS 10 mM)

MCAN			DCAN			TCAN		
C_0 (µg/L)	C_e (µg/L)	q_e (µg/g)	C_0 (µg/L)	C_e (µg/L)	q_e (µg/g)	C_0 (µg/L)	C_e (µg/L)	q_e (µg/g)
59.61	54.80	24.04	250.0	12.94	474.1	250.0	51.71	953.3
157.2	143.2	70.35	500.0	14.35	975.2	500.0	103.4	1871
291.1	245.2	229.6	750.0	16.75	1454	750.0	138.6	3027
488.2	427.6	293.9	1000	19.87	1937	1000	202.6	3834
1056	943.2	551.1	1500	34.84	2907	1250	256.9	4868
TCM			$C_3H_3Cl_3O$			DCAA		
C_0 (µg/L)	C_e (µg/L)	q_e (µg/g)	C_0 (µg/L)	C_e (µg/L)	q_e (µg/g)	C_0 (µg/L)	C_e (µg/L)	q_e (µg/g)
250.0	20.74	1092	250.0	78.56	816.4	68.91	62.81	29.08
500.0	39.47	2236	500.0	135.0	1825	91.89	91.16	3.410
750.0	51.21	3459	750.0	192.6	2759	148.2	176.4	0
1000	82.45	4498	1000	275.5	3623	272.1	303.1	0
1500	144.6	6644	2000	478.7	7175	518.4	579.7	0

Table D-2 Data from adsorption isotherm of three-HANs, TCM, $C_3H_3Cl_3O$, and DCAAs on PAC in single solution (pH 7 and IS 10 mM)

MCAN			DCAN			TCAN		
C_0 (µg/L)	C_e (µg/L)	q_e (µg/g)	C_0 (µg/L)	C_e (µg/L)	q_e (µg/g)	C_0 (µg/L)	C_e (µg/L)	q_e (µg/g)
46.37	37.99	41.07	110.4	1.110	546.6	250.0	41.05	1044
92.42	77.64	72.44	291.7	13.97	1389	750.0	86.98	3282
162.2	128.6	164.4	538.7	25.96	2538	1000	162.2	4189
297.7	258.3	189.3	811.4	38.31	3865	1250	212.2	5189
999.7	893.8	529.7	970.9	42.02	4553	1500	269.9	6150
TCM			$C_3H_3Cl_3O$			DCAA		
C_0 (µg/L)	C_e (µg/L)	q_e (µg/g)	C_0 (µg/L)	C_e (µg/L)	q_e (µg/g)	C_0 (µg/L)	C_e (µg/L)	q_e (µg/g)
500.0	56.22	2133	500.0	215.1	1411	61.86	61.96	0
750.0	122.3	3077	750.0	321.0	2062	63.83	74.93	0
1000	138.9	4305	1000	440.0	2772	95.28	163.6	0
1500	298.5	5889	1500	730.2	3701	306.1	305.1	4.960
2000	557.0	7005	2000	1052	4601	654.1	460.6	904.4

2. Selectivity of adsorption

Table D-3 Data from adsorption isotherms of four DBPs on NR/HMS-SH in mixed solution (pH 7 and IS 10 mM)

DCAN			TCM			$C_3H_3Cl_3O$		
C_0 (µg/L)	C_e (µg/L)	q_e (µg/g)	C_0 (µg/L)	C_e (µg/L)	q_e (µg/g)	C_0 (µg/L)	C_e (µg/L)	q_e (µg/g)
50.73	42.36	41.81	35.36	28.20	35.80	42.82	28.35	72.34
97.73	81.97	77.23	107.6	84.51	113.0	81.19	46.94	167.9
142.7	115.3	137.1	121.9	98.96	114.9	133.8	68.77	324.9
256.2	213.4	207.4	176.7	125.6	248.2	237.7	130.3	521.6
438.8	383.6	275.9	318.5	209.6	544.7	415.9	226.7	946.4
904.6	769.7	667.7	592.8	291.8	1489	839.2	441.4	1969

DCAA		
C_0 (µg/L)	C_e (µg/L)	q_e (µg/g)
73.60	60.07	67.67
196.5	146.3	245.7
267.1	214.0	265.8
513.9	380.6	647.3
3809	1447	11692

Table D-4 Data from adsorption isotherms of four DBPs on PAC in mixed solution (pH 7 and IS 10 mM)

DCAN			TCM			$C_3H_3Cl_3O$		
C_0 (µg/L)	C_e (µg/L)	q_e (µg/g)	C_0 (µg/L)	C_e (µg/L)	q_e (µg/g)	C_0 (µg/L)	C_e (µg/L)	q_e (µg/g)
50.73	15.75	174.9	35.36	22.31	65.22	42.82	22.24	102.9
97.73	18.57	388.0	107.6	37.35	344.2	81.19	39.70	203.4
142.7	27.57	575.7	121.9	59.70	311.3	133.7	68.80	324.7
256.2	60.13	951.5	176.7	112.5	311.6	237.7	140.3	473.1
438.8	85.55	1766	318.5	115.3	1016	415.9	245.1	854.4
904.6	97.13	3997	592.8	412.8	890.9	839.2	436.5	1993

DCAA		
C_0 (µg/L)	C_e (µg/L)	q_e (µg/g)
73.60	57.76	79.22
196.5	148.5	235.4
267.2	200.2	334.9
513.9	421.7	448.0
3809	1605.9	10907

3.   Effect of NOM on DCAN adsorption

Table D-5   Data from adsorption isotherm of DCAN in NOM solution

DCAN in Tap water			DCAN in HPI NOM			DCAN in HPO NOM		
C_0 (µg/L)	C_e (µg/L)	q_e (µg/g)	C_0 (µg/L)	C_e (µg/L)	q_e (µg/g)	C_0 (µg/L)	C_e (µg/L)	q_e (µg/g)
57.49	34.42	112.0	63.55	47.55	76.15	59.55	56.18	16.39
150.9	80.55	341.6	85.18	67.28	88.60	155.5	144.2	55.55
238.9	106.6	636.5	156.3	121.3	163.6	262.9	223.5	193.4
294.3	176.3	572.9	250.9	192.7	285.0	341.7	306.8	170.9
481.0	281.6	968.0	401.1	281.5	580.7	476.9	460.9	7601
			522.5	402.0	568.4			

Table D-6   Data of organic carbon NOM in the solution before and after

adsorption

TOC of Tap water		TOC of HPI NOM		TOC of HPO NOM	
Before adsorption (mg/L)	After adsorption (mg/L)	Before adsorption (mg/L)	After adsorption (mg/L)	Before adsorption (mg/L)	After adsorption (mg/L)
2.869	2.684	3.165	2.855	2.865	1.637
2.833	2.684	3.165	2.979	3.070	1.773
3.090	2.572	3.227	3.289	3.070	1.637
2.906	2.684	2.979	2.668	3.040	2.114
3.127	2.647	3.414	2.668	3.206	1.978

VITA

Miss Yaowalak Krueyai was born on April 11, 1990 in Angthong province. After she graduated high school in Kanchanaphisekwithayalai Suphanburu School, Suphanburi, she studied in Department of Chemistry, Faculty of Science, Chulalongkorn University. She graduated Bachelor's degree of Science in 2011. After that she continued study in Master's degree of science in Hazardous Substance and Environmental Management, Chulalongkorn University.

Some part of this thesis has been published in the 4th International Conference on Environmental Engineering, Science and Management on 27th May to 29th May 2015 at Lotus Hotel Pang Suan Kaew Chiang Mai, Thailand and the 16th IWA UK Young Water Professionals Conference 2015 on 15th April 2015 to 17th April 2015 at Strathclyde University, Glasgow, Scotland.